3. RESULTS:

3.1. General:

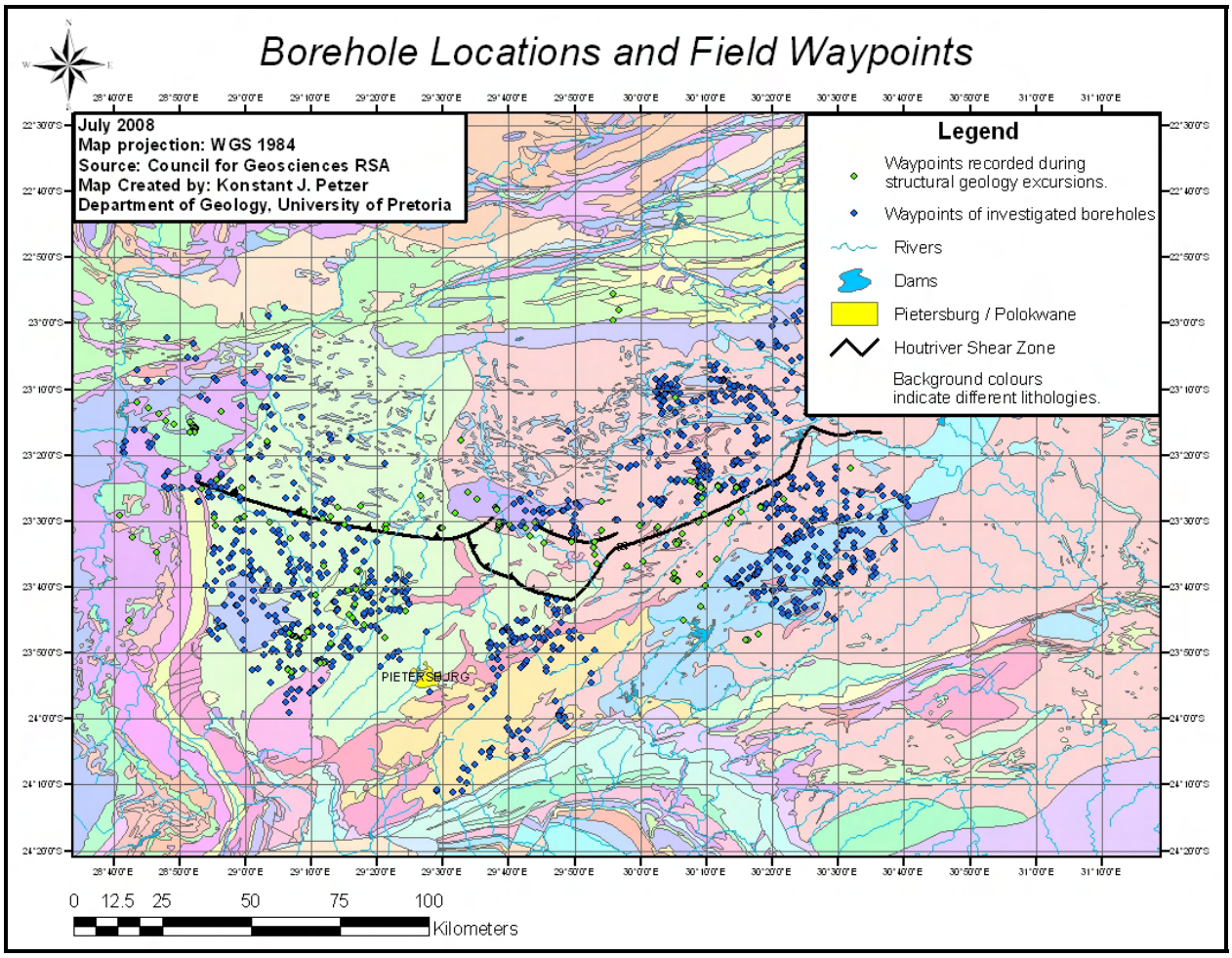

Figure 15: A map showing the location of the boreholes that were analyzed in this study and the waypoints recorded in the field while gathering structural geological data.

3.2. Joints:

JOINTS OVERALL:

Joints play a cardinal role in this project as they are the most common of all the brittle geological structures in the study area. Though joints often form together with faults, the structures described in this section as "joints" refer to the fractures in rocks on which shear displacement (if any) is too small to notice with the unaided eye. Firstly, a combination of dip and strike values were used to construct stereographic projections of the poles of all the measured joint planes (Appendix). Unfortunately, this proved to be less indicative of preferred orientation patterns in three-dimensional space than expected.

Although the overall distribution of joint orientations in the study area is fairly random, some sensible conclusions can still be made from Figure 16, Figure 17 and Figure 18. Firstly, a slight majority of joint strikes are orientated NW-SE and NE-SW. Hypothetically speaking,

NW-SE-striking joints should be favourable for groundwater flow, seeing as the neotectonic tension is NE-SW and should open these joints up (Bird et al. in 2006). Secondly, the NE-SW-striking joints could have been reactivated through strike-slip by the neotectonic stress, causing such joints to also have a water bearing capability. Furthermore, the majority of the joints have steep dips which often indicate formation in a tensional environment (see Anderson's theory in the literature review).

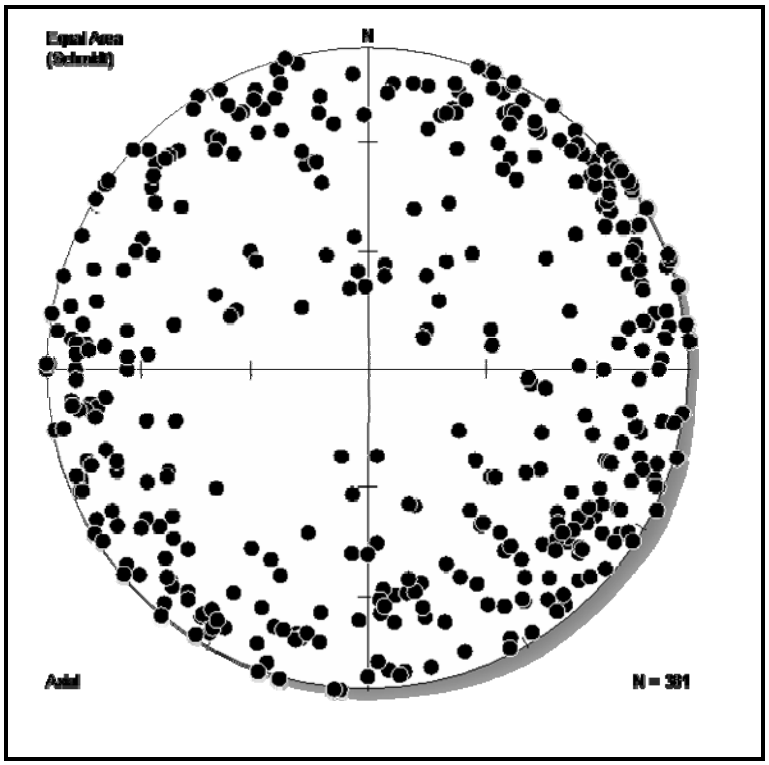

Figure 16: Poles to all joint planes.

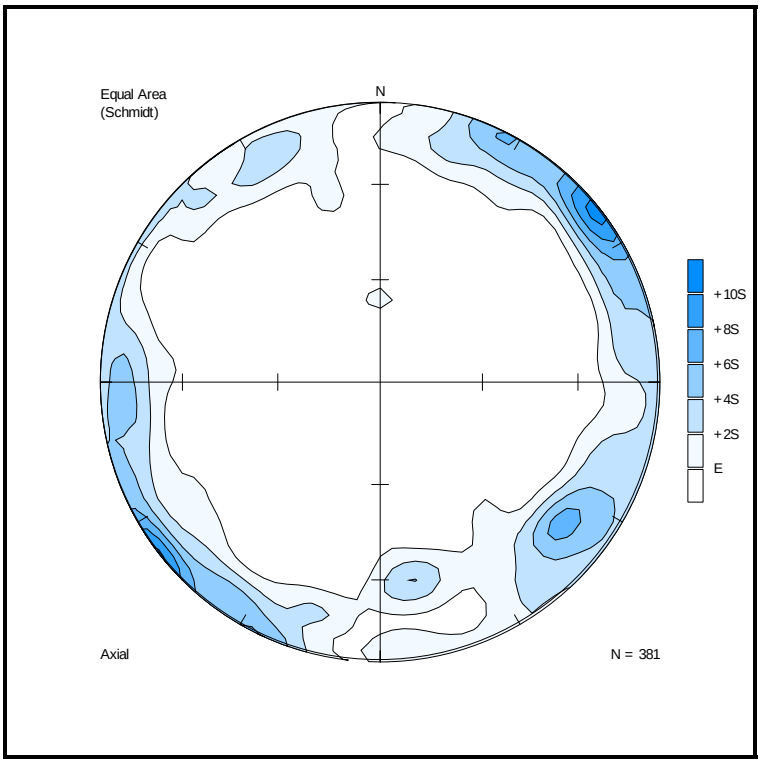

Figure 17: Density distribution of all poles to joint planes.

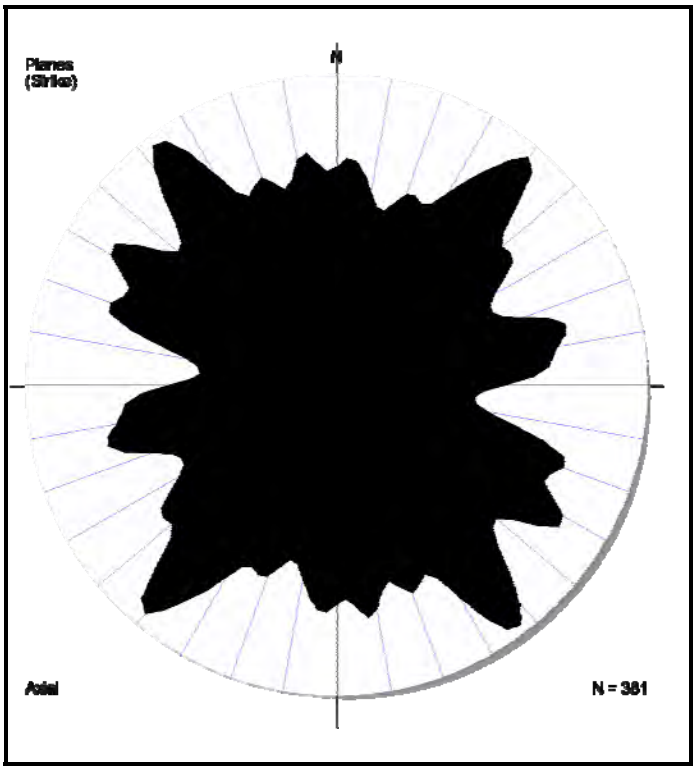

Counting Parameters

Number of Data Points in Set	381
Number of Data Points Included	381
Type of Data	Planes (Strike)
Range of Dip Angles	0° - 90°
Class interval	10°
Class Alignment	Centered at 0°N
Kurtosis, k, of Smoothing Function	206
Half-width of Smoothing Function	±4.7°
Unweighted Calculation	

Frequency Statistics

Mode (Peak)	7.9%
Azimuth Range of Mode	35° - 45°
Smooth Peak	7.6%
Azimuth of Smooth Peak	142.5°
Expected Value, E	5.6%
Standard Deviation	1.7%
95% Confidence Levels	<2.1% & >9.0%

The distribution is statistically uniform.

Figure 18: Rose diagram derived from the strikes of all joint planes.

JOINT INTERSECTION LINEATIONS:

Since no strongly preferred orientation of joints was found locally (i.e. between two or three closely spaced waypoints), the possible existence of another preferred linear orientation was investigated. Lineations along which groundwater flow might be concentrated were calculated from the intersections of joint planes. Theoretically, such intersections can receive water from the two or more joints creating it. The orientation of these linear intersections were plotted stereographically and analyzed for their density distribution on contoured stereographic projections (see Figure 115 to Figure 139 in the appendix). Unfortunately, this exercise also proved inconclusive, since no dominant preferred three dimensional orientation was found regionally from the intersection lineations. Nevertheless one can draw the conclusion that most of the intersection lineations are steeply inclined (making them difficult targets for drilling, but important for the infiltration of surface water) and it appears that a small majority of intersection lineations plunge towards the northwest. Unfortunately, the total amount of intersections was too large for Spheristat2.2 to plot on a single stereographic projection and therefore the intersections were once again plotted on individual 10' x 10' blocks of latitude and longitude (Figure 115 to Figure 139 in appendix). On a more local scale, the following stereographic projections did show some clustering of sub-horizontal intersection lineations: S23˚ 20' E28˚ 50' (SSE); S23˚ 30' E29˚ 20' (NE-SW); S23˚ 40' E30˚ 00' (NW); S23˚

40’ E30˚ 10’ (NW-SE and SW); S23˚ 50’ E29˚ 10’ (NE- SW). Due to their sub-horizontal nature the trends of these clusters are closely related to the major strike directions of the joints that formed them (true for most of the blocks mentioned). It is also worthy to note that the rivers that occur in the blocks mentioned flow parallel to the trend of the sub-horizontal clusters of joint intersects.

JOINT STRIKES:

It was decided to simplify the joint orientation investigation to two dimensions by constructing rose diagrams of the joints’ strikes. Even at a local scale, very few joint sets showed a definite preferred orientation in their strike, and/or matched the preferred orientation of joints at an adjacent waypoint. In Figure 19, the strikes of the joints were grouped together in 10’x10’ blocks on the geology map and plotted onto rose diagrams to determine the major strike directions for each block. The individual rose diagrams can be seen in the appendix. From Figure 19, it quickly becomes apparent that most joints are not confined to lithological boundaries and that the events that caused the joints usually had similar structural effects throughout a certain area, regardless of the lithologies encountered during that event. Consequently, it was decided not to describe the distribution of joints in terms of their lithological location, but rather to relate their spatial distribution to a known regional feature such as the Hout River Shear Zone.

In Figure 19 the rose diagrams indicating the strikes of joints have been spatially represented on a geology map. Each of these rose diagrams were colour coded according to the major strike directions in that specific 10’x10’ block. Due to the lack of outcrops and accessibility, the whole map could not be covered in 10’x10’ rose diagrams, but nonetheless the data available is fairly well spread over the study area. Although this is not the most statistically correct method for orientation interpretations, it does help to quickly identify and group major strike directions of joints in the study area. In this way, if any patterns are observed at a quick glance, it is easy to compare the patterns to the spatial representation of transmissivity and sustainable yield values at a later stage in the investigation.

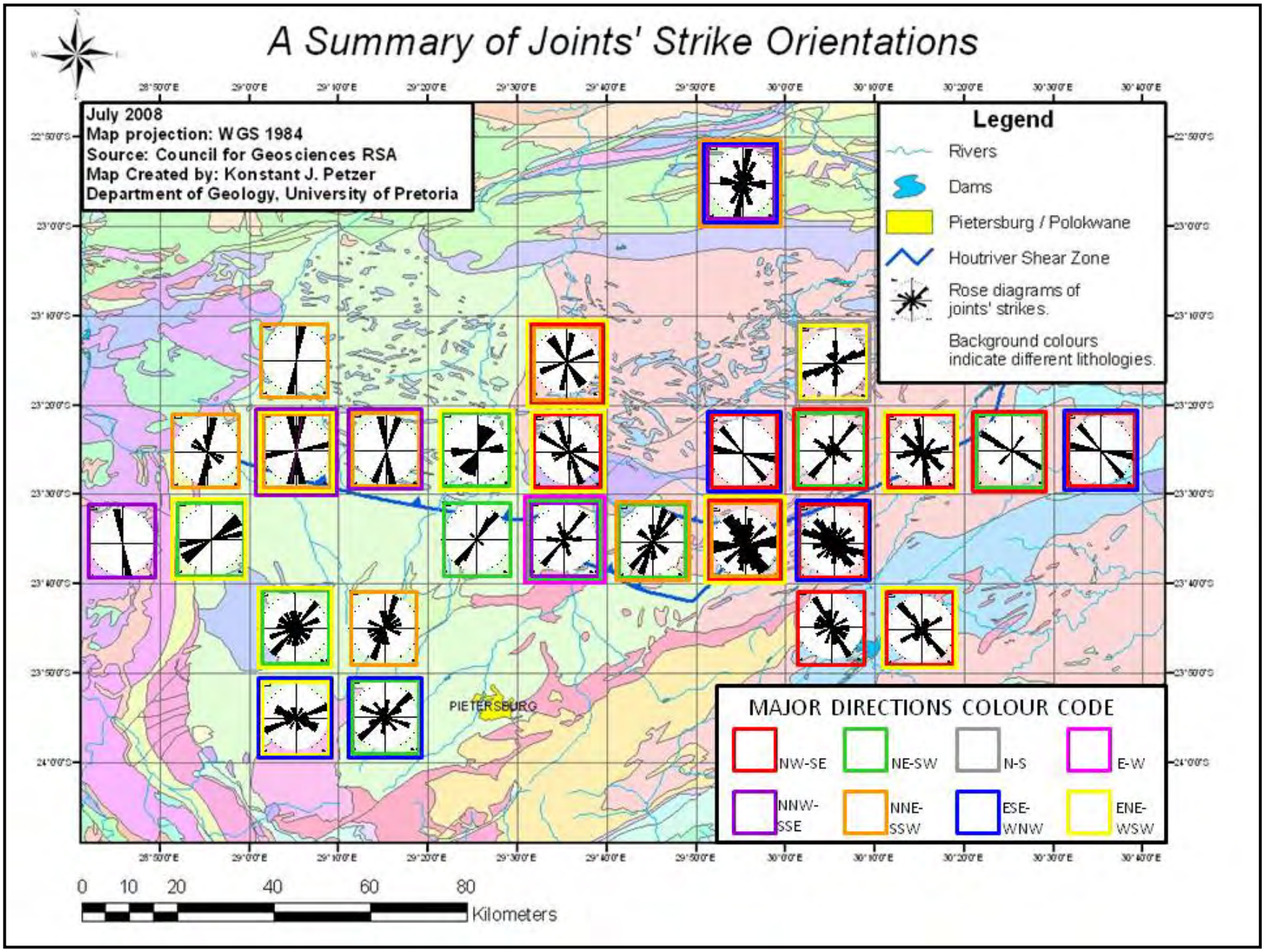

Figure 19: A map summarizing the major strike directions of joints in each 10' x 10' block that yielded field measurements.

Figure 19 shows that the NE-SW striking joints are predominantly found in areas south of or on the Hout River Shear Zone (HRSZ). Apart from the fact that NE-SW joints could have been reactivated as strike-slip faults, they also run parallel to the major dyke swarms of the area which might add an additional advantage in terms of groundwater storage or flow due to compartmentalisation of the aquifers. Unlike the NE-striking joints, areas with major joint strikes orientated approximately N-S were mostly found to the north of the HRSZ. NW-SE striking joints are reasonably continuous throughout the centre of the map in a NW-SE line and also towards the east of the study area. This might mean that the NW-SE striking joints are the most penetrative (i.e. have the longest extent) and that some of the same joints were recorded at more than one locality. If this assumption holds true, the NW-SE trending joints are once again likely to be favourable conduits for groundwater. However, with a lack of outcrop and generally limited exposure, it is difficult to establish the lateral extent of joints. Despite being the most penetrative, NW-striking joint sets run perpendicular to most of the other structures observed in the area (such as dolerite dykes; Figure 7). Since the NE-trending structures cross-cut the NW-trending joints, the theory that these joints are favourable pathways for groundwater might be invalid. Perhaps the intersections of the NW-trending joints and the perpendicular structures blocking these joints are worthy targets for groundwater, but this has yet to be demonstrated through more precise drilling in the future. If the dykes that intersect the NW-striking joints are themselves conduits for groundwater, as they often are, the intersections of these features would especially be worth investigating. Lastly, East-northeast (a direction demonstrated by many of the geological structures in the area, including the LB) is one of the other strike directions of joint planes fairly commonly recorded throughout the study area.

It is important to note that just because certain joint orientations are dominant doesn't necessarily mean that these joints are better groundwater conduits than others. The considerable number of variables controlling groundwater flow/occurrence does not require a direct relationship between dominant joint orientation and flow direction to exist. Minor joint sets or other secondary structures may also be important conduits.

JOINT GROUPS BASED ON DIP ANGLES:

After investigating all joints jointly, it was decided to divide the joints up into groups based on their respective dip angles. The reason for this subdivision is the fact that different dips in joints and shear joints are mostly the result of different stress/strain regimes during times of formation (Anderson's Theory). Figure 20 shows a rose diagram of joints with shallow dip angles, ranging from 0˚ to 45˚. According to Anderson (1951), shallow dips (~30˚ from horizontal) are the result of thrusting, where σ_3 is vertical. If one disregards the formation of permeable mylonite during thrusting and only consider the stress/strain conditions at

work, compressional thrust faults and their associated joints are less favourable for groundwater exploration than their tensional counterparts.

Table 3: Measured joint quantities. (* Sum not exactly equal to 100% due to rounded averages)

Dip angle of joints	Comment	Amount of joints	Percentage
Shallow (0˚ - 45˚)	Usually thrust (compression) induced or decompressional	36	9.45%
Moderate (46˚ - 79˚)	Usually tensionally induced	188	49.34%
Steep (80˚ - 90˚)	Strike-slip, or Mode I tensional joints	157	41.21%
All joints (0˚ - 90˚)		381	100% *

Of all the measured joints, the shallow dipping ones were by far the least common. Even though the statistical distribution on the rose diagram (Figure 20) was once again uniform, a majority of shallow angle joints striking NE-SW does exist. Thrusts striking NE-SW are possibly from Neoarchaean times, as many of the tectonic features from this time have north-eastern trends. Moreover, older thrusts with NE strikes also exist from when the Pietersburg- and Giyani Greenstone Belts formed (De Wit et al., 1992). There is also a minor NNE-SSW strike present among the shallow joints, possibly from the $\mathbf{D_1}$ event mentioned by Passeraub et al. (1999) prior to formation of the HRSZ, or from the Limpopo Orogeny. Sub-horizontal joints can also form by dilatation (pressure release i.e. by means of erosion) or as cooling joints of plutons. The distribution of shallow-dipping joints is fairly well spread over the study area, implying that the whole area was likely subjected to compression at one time or another, with σ_1 orientated horizontally (see Figure 21).

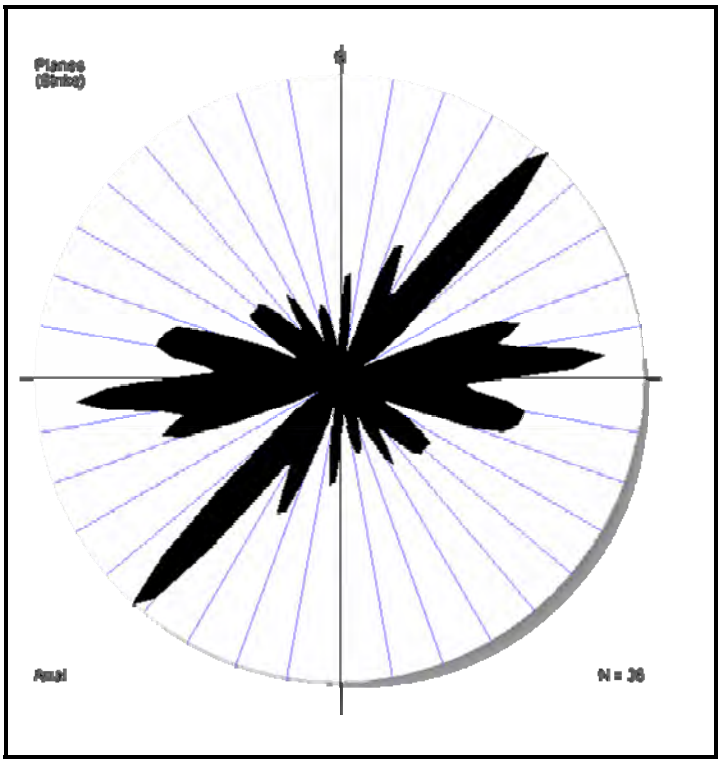

Counting Parameters	
Number of Data Points in Set	36
Number of Data Points Included	36
Type of Data	Planes (Strike)
Range of Dip Angles	0° - 45°
Class interval	10°
Class Alignment	Centered at 0°N
Kurtosis, k, of Smoothing Function	206
Half-width of Smoothing Function	±4.7°
Unweighted Calculation	

Frequency Statistics	
Mode (Peak)	13.9%
Azimuth Range of Mode	35° - 45°
Smooth Peak	15.1%
Azimuth of Smooth Peak	42.5°
Expected Value, E	5.6%
Standard Deviation	5.6%
95% Confidence Level	>16.8%

The distribution is statistically uniform.

Figure 20: Rose diagram derived from the strikes of shallow-dipping (0˚ - 45˚) joints.

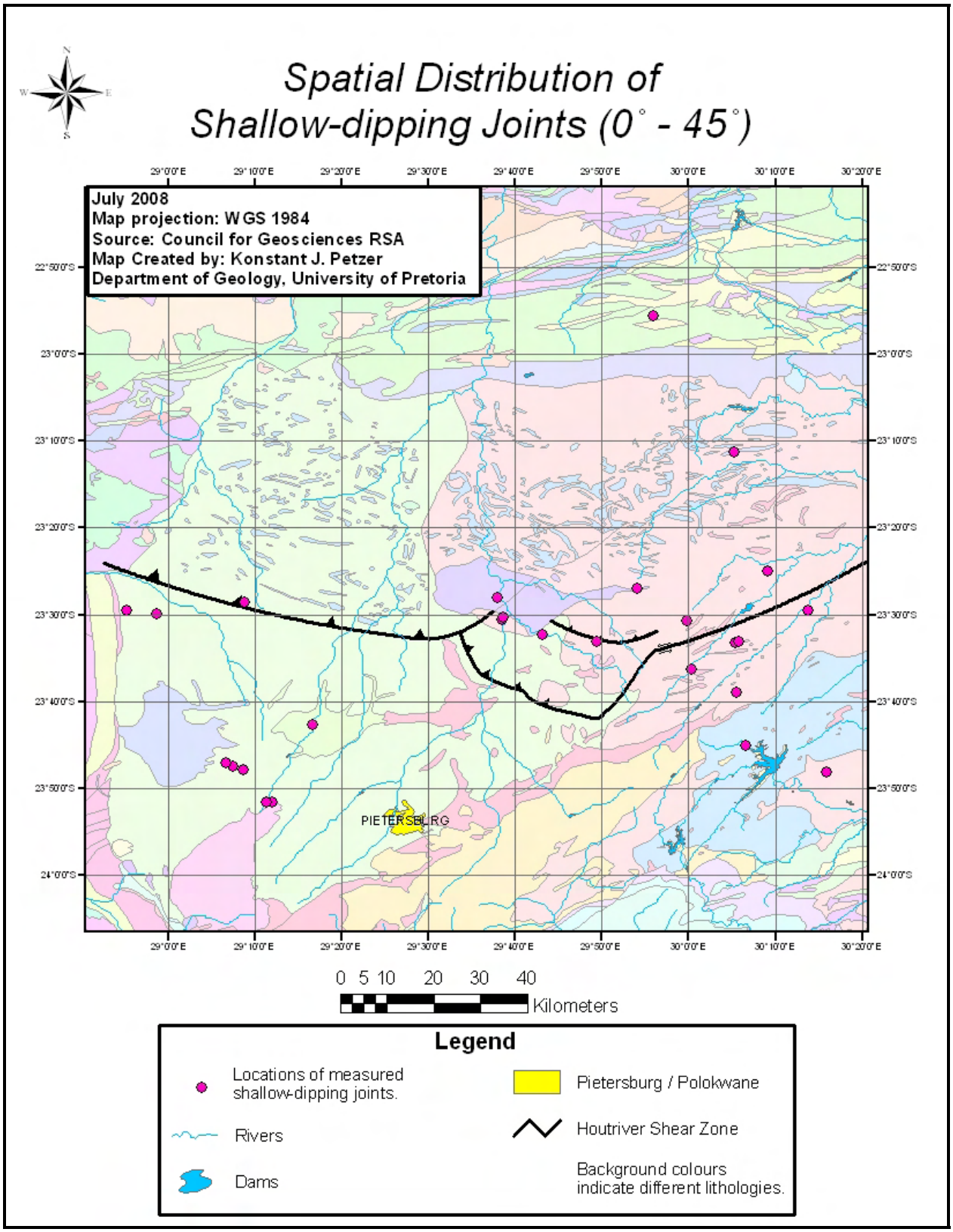

Figure 21: A map showing the spatial distribution of shallow-dipping joints that were measured. Note that the distribution of shallow dipping joints is not confined to one specific measured area on the map.

Moderately dipping joints (46˚ – 79˚) were investigated in Figure 22. This range of dips includes the dips formed during normal (or reverse) faulting (~60˚ dip). Normal faults and their associated joints form in a tensional regime in which σ_1 is vertical and S_1 is perpendicular to strike (Anderson, 1951). Theoretically, joints that formed under these conditions are the most suitable joints in the search for groundwater due to their dilation property. When looking at Figure 23 one can see that the distribution of azimuths for moderately dipping joints is statistically uniform. Only a slight majority of moderately dipping joints (9.6%) are striking NE-SW. Since no clear preferred orientation was found in the strikes of the moderately dipping joints it was decided to investigate the ones that are orientated sub-parallel to the more recent tectonic regimes (Karoo and Neotectonic regimes). Moderately dipping joints that strike approximately E-W (perpendicular to the N-S extension that occurred during the breakup of Gondwana), as well as those that strike approximately NW-SE (perpendicular to neotectonic extension) are both spread out quite uniformly over the study area, but are mainly found south of the HRSZ (See Figure 19 and Figure 23). However, it might only be the lack of outcrop north of the HRSZ that lead to this observation.

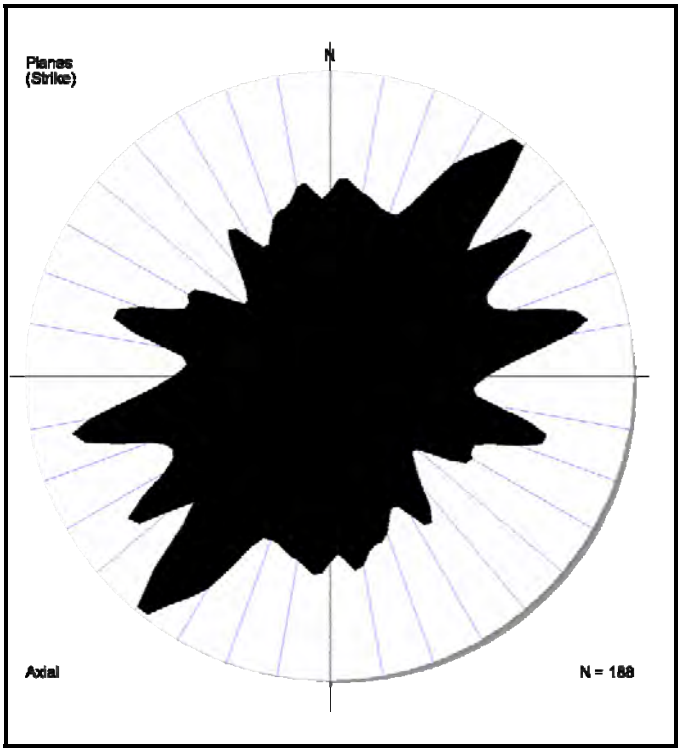

Counting Parameters

Number of Data Points in Set	188
Number of Data Points Included	188
Type of Data	Planes (Strike)
Range of Dip Angles	46˚ - 79˚
Class interval	10˚
Class Alignment	Centered at 0˚N
Kurtosis, k, of Smoothing Function	206
Half-width of Smoothing Function	±4.7˚
Unweighted Calculation	

Frequency Statistics

Mode (Peak)	9.6%
Azimuth Range of Mode	35˚ - 45˚
Smooth Peak	8.9%
Azimuth of Smooth Peak	40.0˚
Expected Value, E	5.6%
Standard Deviation	2.5%
95% Confidence Levels	<0.6% & >10.5%

The distribution is statistically uniform.

Figure 22: Rose diagram derived from the strikes of moderately dipping (46˚ - 79˚) joints.

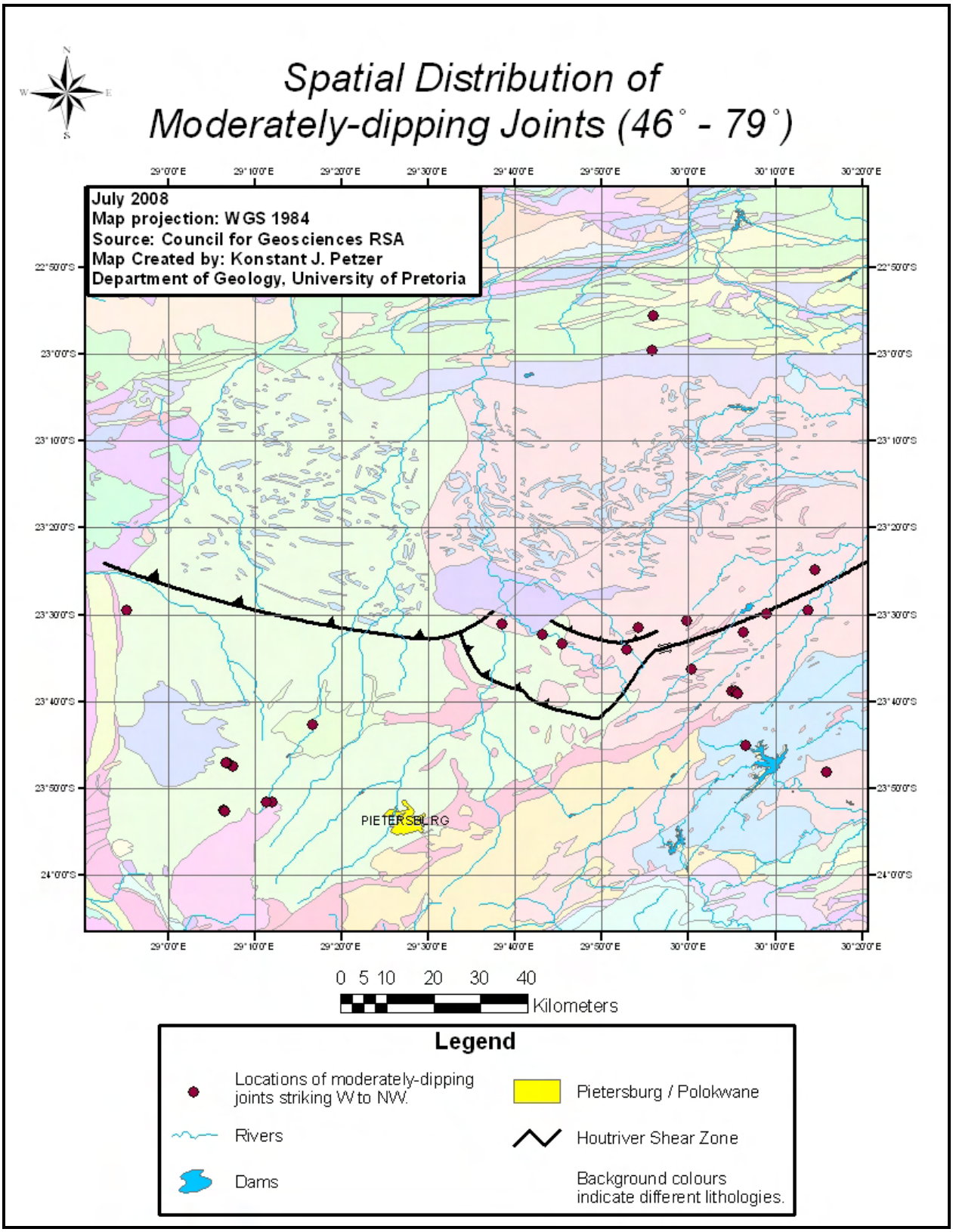

Figure 23: A map showing the spatial distribution of measured joints with moderate dip angles and strikes between W and NW. The distribution of moderately-dipping joints is slightly concentrated on the eastern side of the study area, but still fairly dispersed over all the measured areas.

The last group of joints are sub-vertical to vertically dipping (80˚ - 90˚) which are either strike-slip shear joints or mode I tensional joints. Strike-slip faults and their associated joints form when σ_2 is vertical (Anderson, 1951). However, since no shear displacement was noticed in these joints, the majority of the steep joints measured are classified as mode I tensional joints. Once again, the "opening up" property of these joints is what makes them sought after as possible conduits for the flow of groundwater. Unlike the other groups of joints, the steep joints did show a statistical preferred orientation striking NW-SE, as seen on the rose diagram in Figure 24. Then again, just as the joint groups discussed previously, the steep joints also show a uniform spatial distribution over the study area and are not concentrated in a specific area (see Figure 25). Due to their strike, the steep joints in the area likely formed under neotectonic stress conditions and show potential for groundwater.

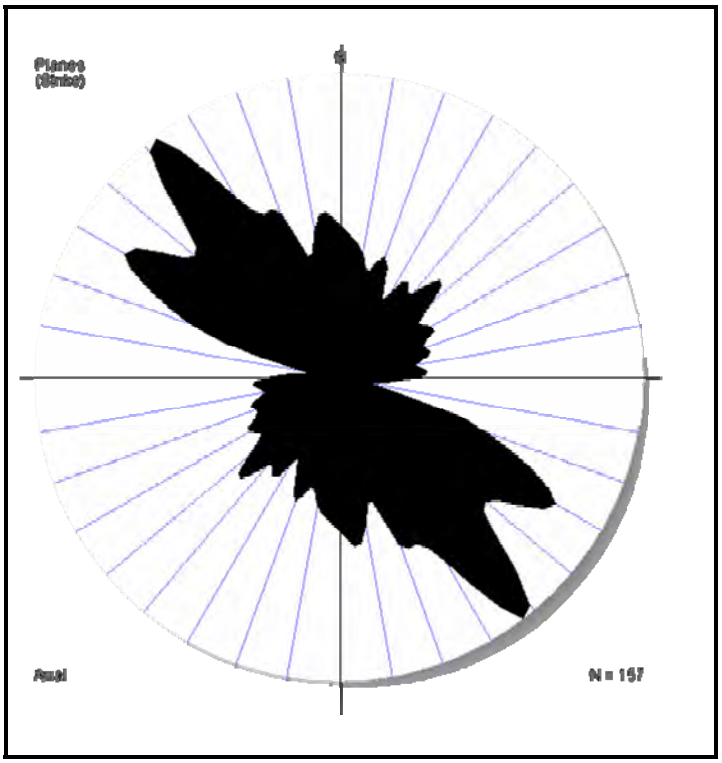

Counting Parameters

Number of Data Points in Set	157
Number of Data Points Included	157
Type of Data	Planes (Strike)
Range of Dip Angles	80° - 90°
Class interval	10°
Class Alignment	Centered at 0°N
Kurtosis, k, of Smoothing Function	206
Half-width of Smoothing Function	±4.7°
Unweighted Calculation	

Frequency Statistics

Mode (Peak)	12.1%
Azimuth Range of Mode	135° - 145°
Smooth Peak	12.0%
Azimuth of Smooth Peak	142.5°
Expected Value, E	5.6%
Standard Deviation	2.7%
95% Confidence Levels	<0.2% & >10.9%

The distribution has a preferred trend.

Figure 24: Rose diagram derived from the strikes of steeply dipping (80˚ - 90˚) joints.

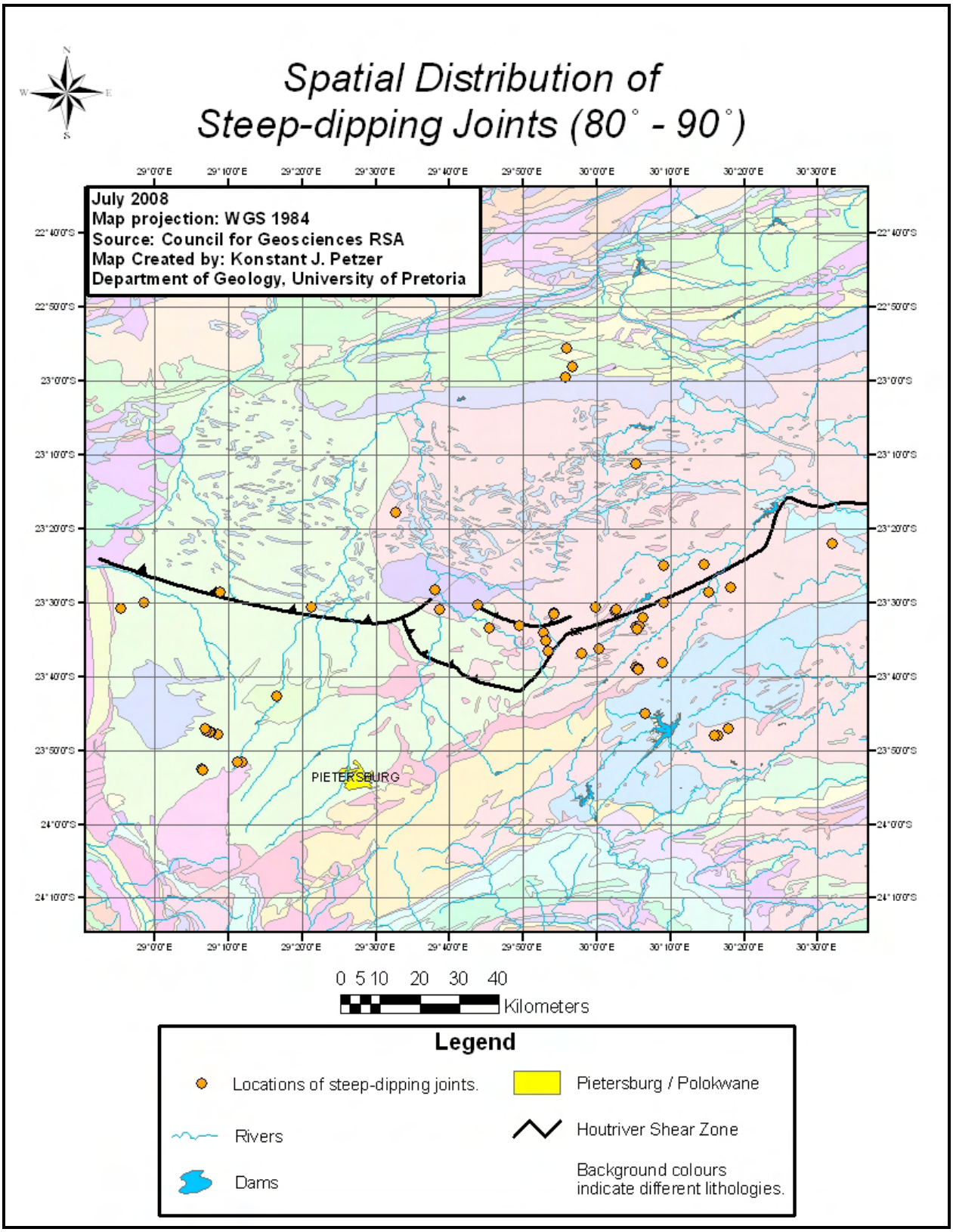

Figure 25: A map showing the spatial distribution of measured joints with steep dip angles. Steep-dipping joints are the most uniformly distributed spatially throughout the study area.

It is essential to note that not all joints will exactly meet the description of the joints described above and that combinations of joints may also occur. Often, joints are formed due to simultaneous lateral and vertical forces acting on a rock in which case a combined name such as “normal dextral fault” is used to describe it. However, as mentioned before, this section only deals with joints in which displacement is too small to notice. Thus the joints were only grouped based on their angle of dip and not on their sense of movement, as this will be discussed under the section for faults.

Figure 26: A Google Earth satellite image of the eastern margin of the Waterberg Group (the western boundary of the study area). Note how clearly visible the NE, E and SSE-striking joints are in the supracrustal rocks of the Waterberg and how these joints dissipate in the basement lothologies on the east.

Figure 27: Slightly weathered gneiss with well-preserved joint sets.

3.3. Faults and shears:

FAULTS AND SHEARS GENERAL INFORMATION:

Although not quite as common as joints, faults are invaluable to the study of structural geology and its relevance to the flow of groundwater. The same principles of groundwater flow in joints are also applicable to faults. Larger, brittle faults that contain brecciated material are especially favourable settings for groundwater movement and normal faults might be of great interest to this study, as they represent extension. Of all the faults observed in the field, N-S and WNW-ESE striking faults were most common, followed by NE-SW and ENE-WSW striking faults. However, as mentioned before, there is a lack of outcrops in certain parts of the study area and therefore only a few faults could be identified and measured. Besides the lack of outcrop, the lack of positive topography displayed by pre-tectonic lithologies made the task of identifying the vertical sense of movement of faults extremely difficult. In fact, only a handful of faults could be classified based on their vertical movement (not nearly enough for any statistical conclusions to be drawn) so the faults were compared to one another more on the basis of their lateral sense of movement. This is one of the main reasons why the author decided to divide the joints up into different groups based on their dip angles. In fact, all the information discussed under the section for joints (section 4.1) can be considered under this section for faults, because most of the principles of formation are identical for both these types of structures.

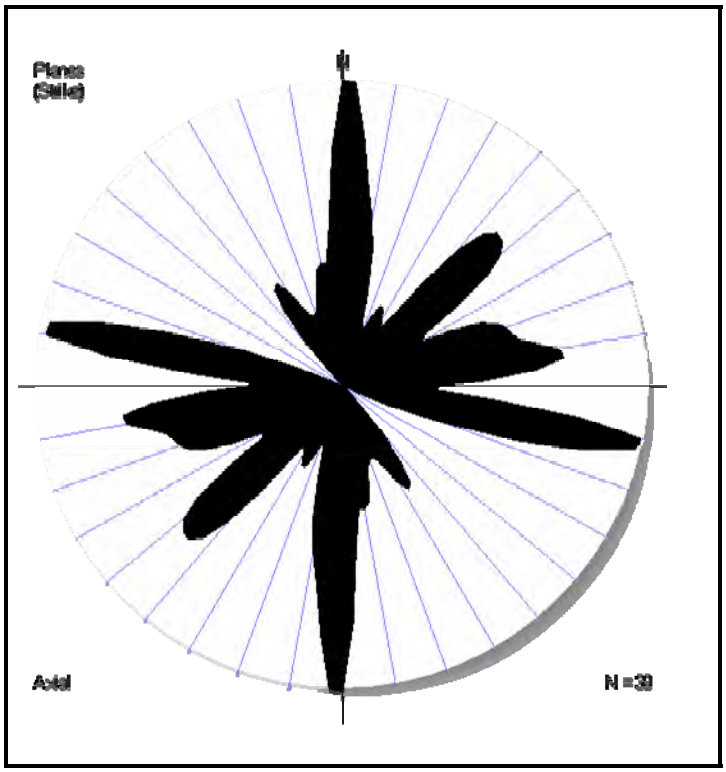

Counting Parameters	
Number of Data Points in Set	39
Number of Data Points Included	39
Type of Data	Planes (Strike)
Range of Dip Angles	0° - 90°
Class interval	10°
Class Alignment	Centered at 0°N
Kurtosis, k, of Smoothing Function	206
Half-width of Smoothing Function	±4.7°
Unweighted Calculation	

Frequency Statistics	
Mode (Peak)	12.8%
Azimuth Range of Mode	-5° - 5°
Smooth Peak	13.2%
Azimuth of Smooth Peak	0.0°
Expected Value, E	5.6%
Standard Deviation	5.4%
95% Confidence Level	>16.4%
The distribution is statistically uniform.	

Figure 28: Rose diagram derived from strikes of faults observed in the field.

In order to better grasp the spatial distribution of faults in the area of interest, geophysical data (aerial magnetic survey) was acquired to look for the displacement of dykes and other features as an indication of faulting. Unfortunately this method also mainly looks at lateral displacement (of dykes in this case) and it is uncertain whether all the normal and reverse faults, as well as faults parallel to the dolerite dykes were properly detected. It was also found that the data supplied by the Council for Geoscience of South Africa only covers patches of the total study area. By using the aerial magnetic data available, it appears as if the regional scale faults found in the basement lithologies mostly strike NW-SE (Figure 29), except in the Giyani Greenstone Belt region, where the regional faults mostly strike NE-SW. One must remember that the majority of dolerite dykes in the area strike NE or NNE, which could have made it more difficult to detect NE-SW striking faults.

Once again, when taking into consideration the neotectonic stress/strain directions (NE extension and NW compression; Bird et al., 2006), the NW- trending faults may be worthy targets for groundwater exploration. Faults that are sub-parallel to the extension direction (NE-SW) could also have been reactivated by strike-slip, which means that such faults can't be excluded as targets for groundwater.

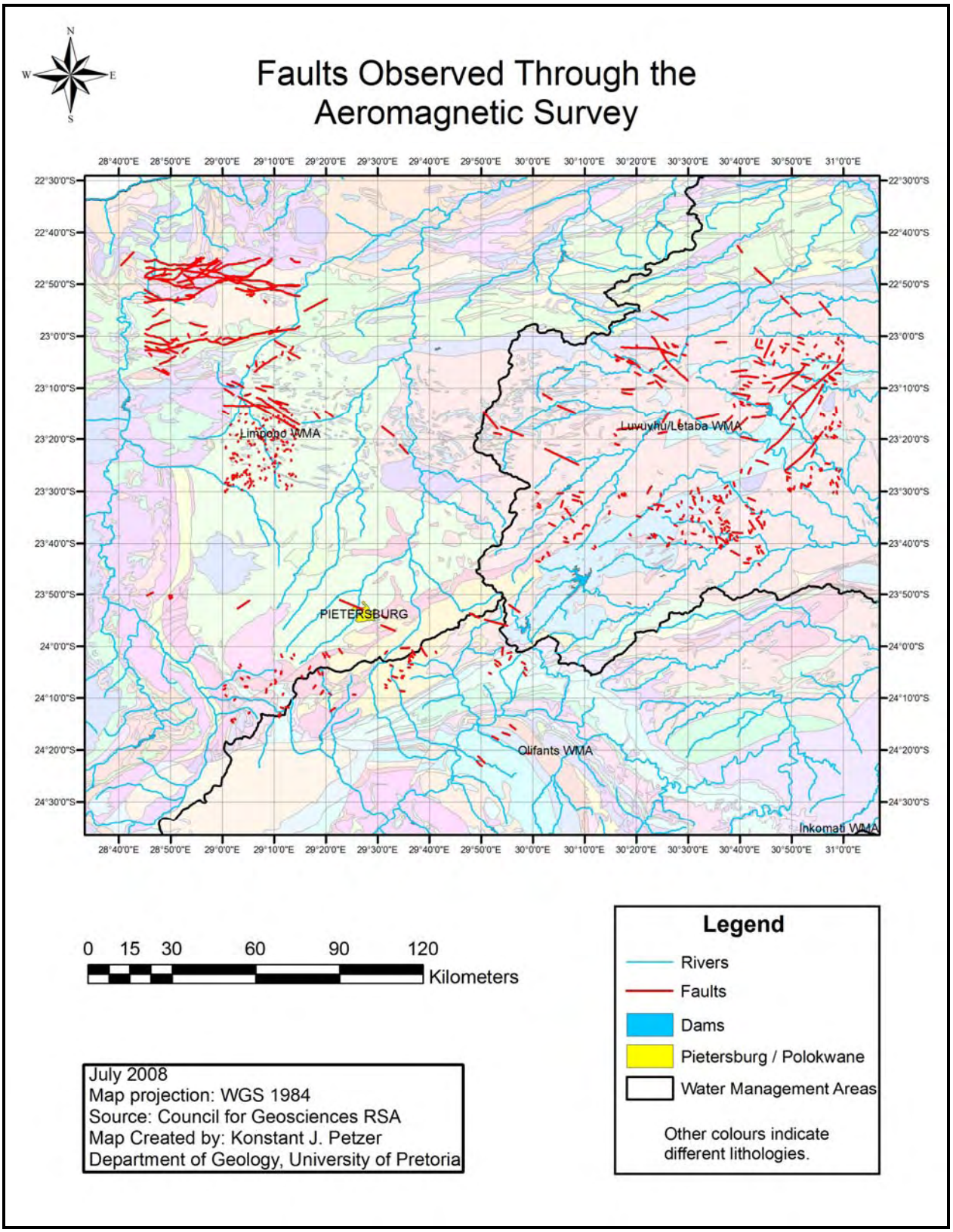

Figure 29: A map indicating some of the faults in the study area that were observed through an aeromagnetic survey by the Council for Geosciences of South Africa.

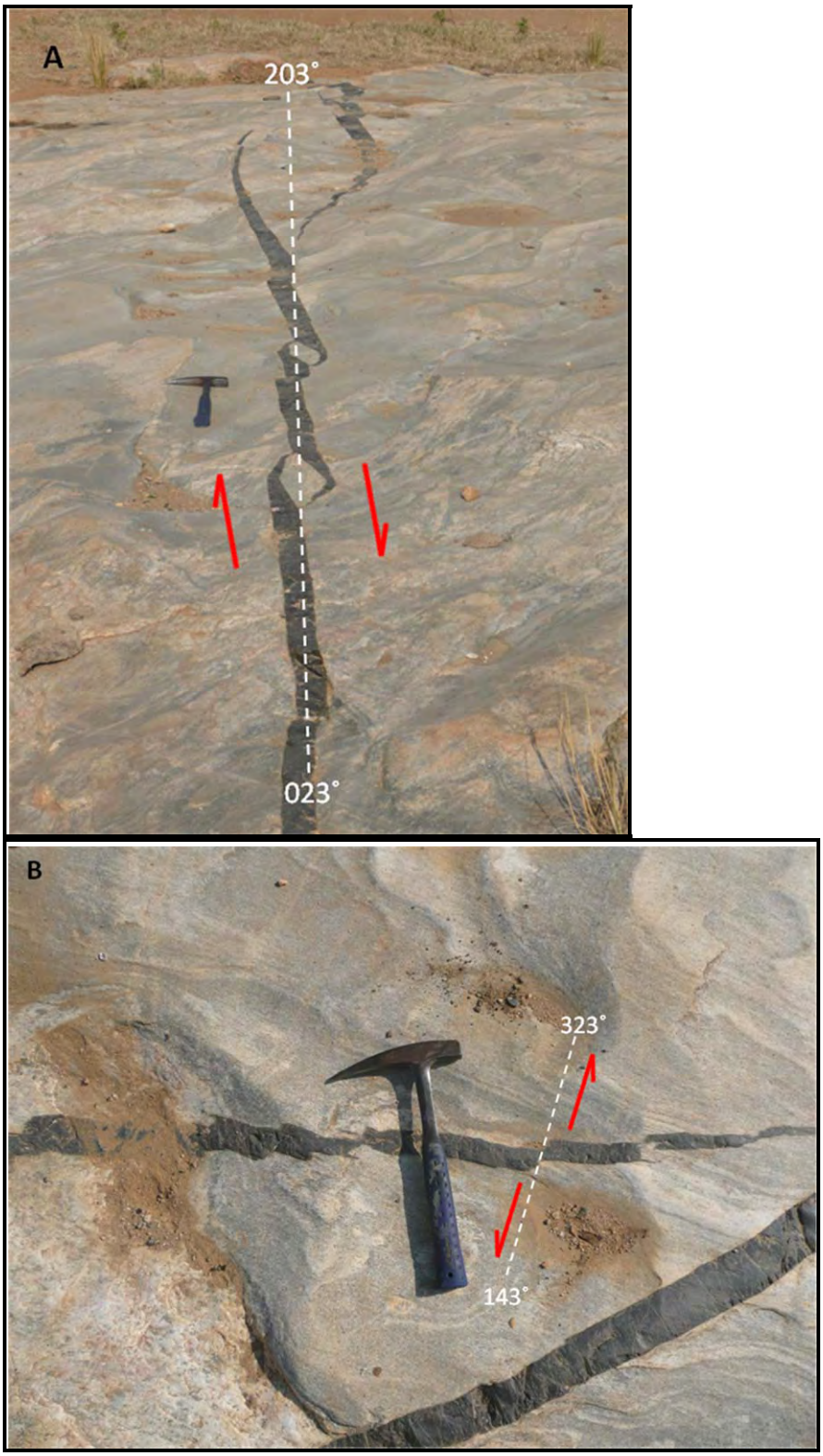

Figure 30: Near the township of Middelwater is an interesting outcrop of migmatite containing some joints, dolerite stringers, and evidence for a few episodes of shearing. (A) In this figure an episode of dextral shear caused the dolerite stringer to form characteristic "pull-apart" formations in the dolerite stringer. The azimuth of this shearing event is slightly offset from the original azimuth of the dolerite stringer, indicated in white. (B) A later event caused step-like sinistral shear in the dolerite stringers along a different orientation.

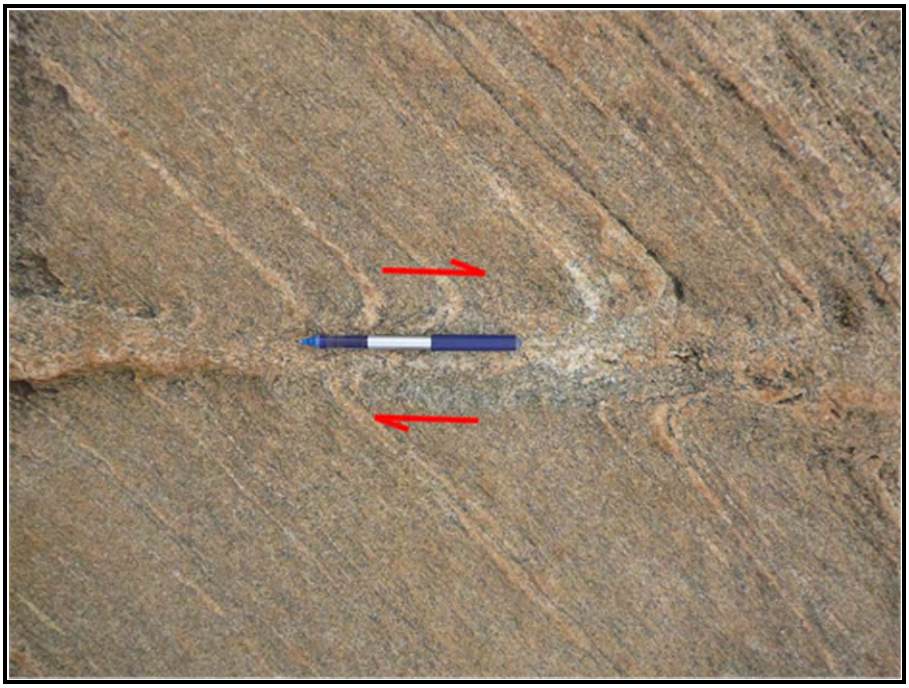

Figure 31: Dextral shear in a banded granitoid.

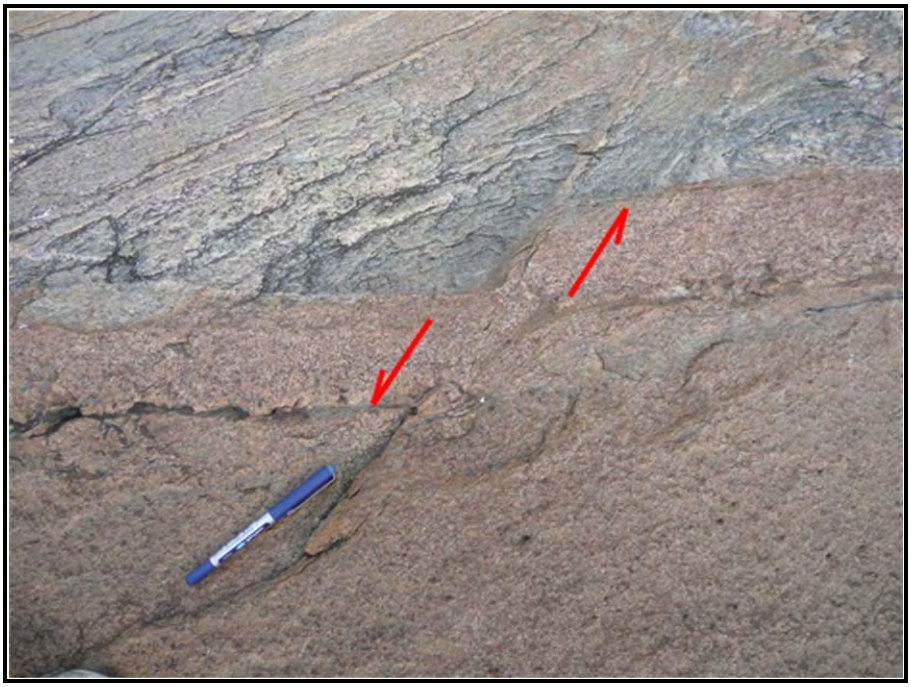

Figure 32: A small sinistral fault shown by the displacement of a pegmatite vein in granitic gneiss.

THE HOUT RIVER SHEAR ZONE:

According to Perchuk (2000) the Hout River Shear Zone can be up to 5km wide in some areas. With that in mind, it was decided to build a 2.5km buffer (a locus of all points on the topographical surface that are 2.5km and closer from the HRSZ) around the approximate location of the HRSZ (on ArcGIS 9.2) so that the total width of the buffer is equal to 5km (Figure 33). Boreholes that fall within the HRSZ buffer demonstrated a higher average transmissivity value than that of the boreholes outside of the buffer, but the average sustainable yield value within the buffer proved to be less favourable than the average value from the rest of the boreholes (refer to Table 4). Considering the tremendous amount of displacement undergone by the HRSZ (vertical displacement of up to 15km; Miyano et al., 1992; Perchuk et al., 1996), it comes as no surprise that the transmissivity in the buffer is above average. The displacement along the shear planes most definitely would have formed more rocks such as mylonite (at greater depths under brittle-ductile conditions) and cataclasite (at shallower depths under brittle conditions). Brittle reactivation along the shear zone could also have converted mylonite into more permeable cataclasite, which could ultimately be responsible for the high transmissivity readings. A lower average of sustainable yield within the HRSZ could be due to a number of factors. The author suspects that the high transmissivity, combined with the geometry of the HRSZ might actually be some of the culprits causing the low Q-values in the following manner: Previous studies have shown that the HRSZ is a relatively steep structure that extends to deep crustal levels (for example Smit et al., 1992). Therefore, surface water and groundwater probably infiltrate and descend quickly (high transmissivity and strong pull by gravity down a steep angle) along the HRSZ to very deep levels that lie beneath the average drilling depth for water exploration. However, very few of the available borehole entries fall within the buffer created and therefore the T and Q relationships found will have to be substantiated by more data.

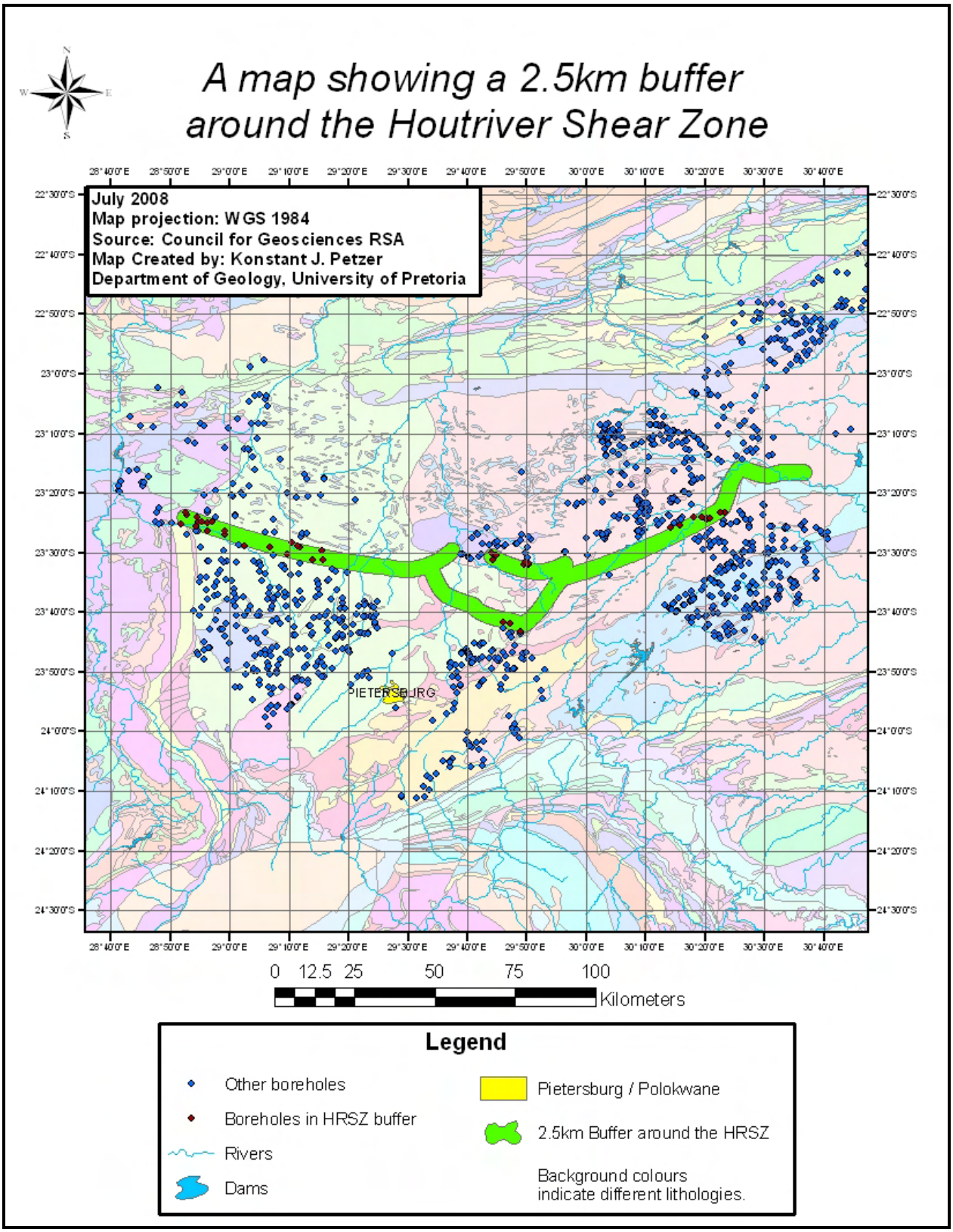

Figure 33: A map showing a 2.5km buffer around the Hout River Shear Zone (i.e. 5km wide) and the boreholes that fall within that buffer. Unfortunately not many of the boreholes that were analyzed fall within the buffer. Nonetheless, the mean average T-value of these boreholes did prove to be slightly higher than the average T-value of those outside of the buffer but that same relationship was not shown in the average Q-values.

Table 4: The mean average T and Q values from inside and outside of the 2.5km buffer around the Hout River Shear Zone.

	Mean Average Logan Transmissivity (T) $m^2/24hr$	Mean Average Yield (Q) L/sec./24hr
Inside HRSZ Buffer	47.33	1.08
Outside HRSZ Buffer	42.83	1.17

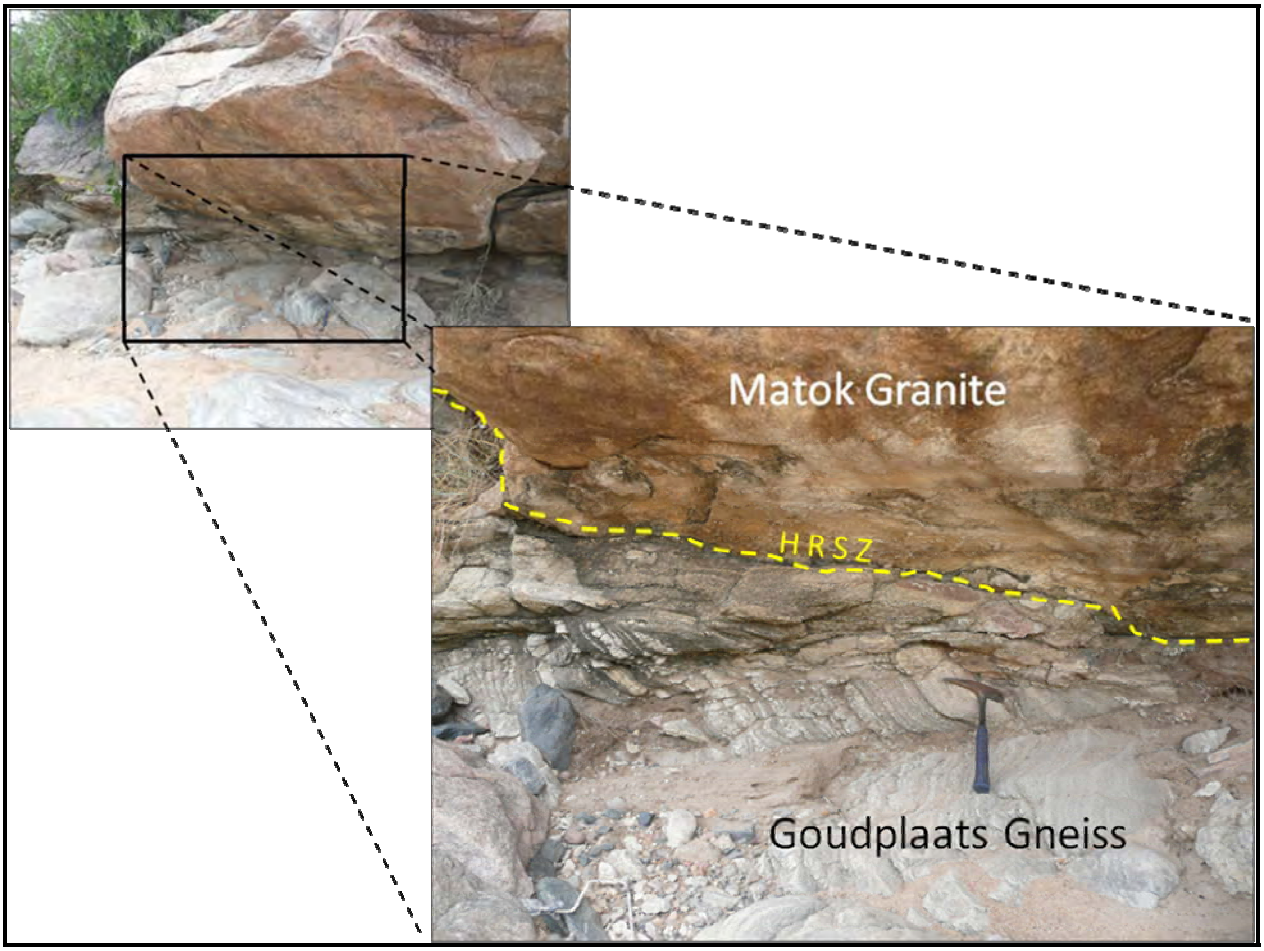

Figure 34: An outcrop showing a small part of the HRSZ between the Matok Granite and the Goudplaats Gneiss.

3.4. Folds:

When rocks are folded, dilational openings and longitudinal joints sometimes form along the hinge lines of the folds due to flexural slip and strain compensation. Since water usually flows following the path of least resistance (but under the influence of gravity) these hinge lines could act as conduits for groundwater flow. However, not many of the hinge lines observed in the field showed signs of longitudinal joints and therefore other brittle structures are still favoured over hinge lines for groundwater exploration. Hinge lines measured in the field are dominantly trending E-W to ESE-WNW. It is likely that the majority of the folds were formed through the D_1 and D_2 events recorded in the HRSZ by Smit et al. (1992) or by the 2.0 Ga. southward-verging reactivation event of the Palala Shear Zone mentioned by Bumby et al. (2004). Furthermore, there are also a number of folds with hinge lines trending approximately NE-SW, possibly as a result of the NW-vergent thrusting between the Pietersburg- and Giyani greenstone belts or the NW-SE compression related to the Wegener Stress Anomaly described by Bird et al. (2006), depending on the age of the folds.

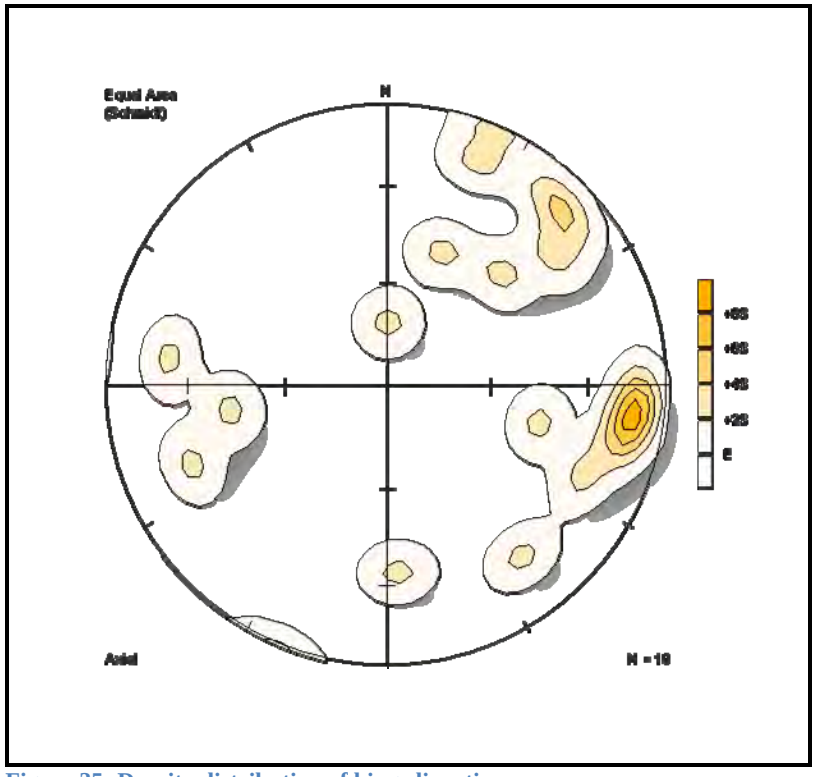

Figure 35: Density distribution of hinge lineations.

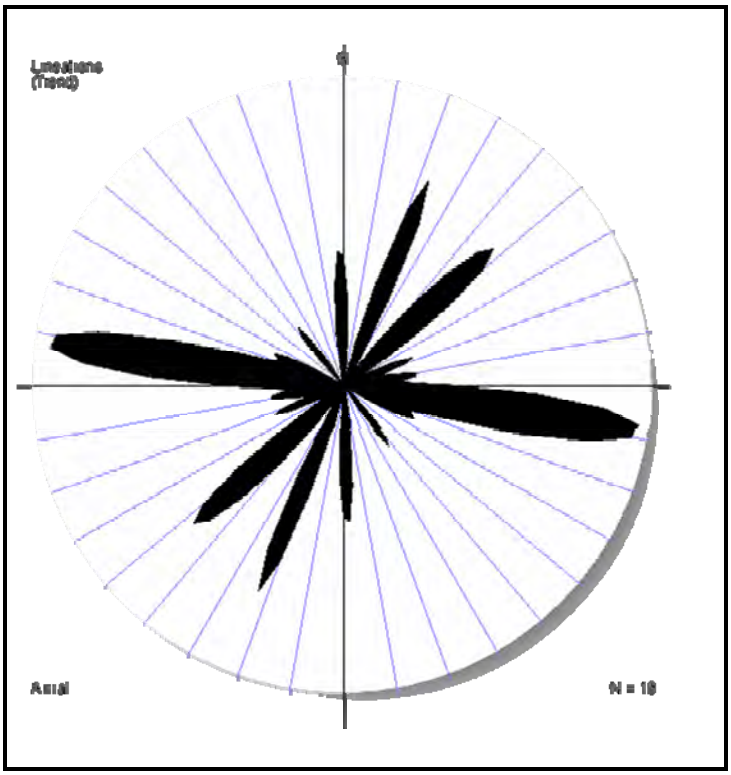

Counting Parameters

Number of Data Points in Set	19
Number of Data Points Included	19
Type of Data	Lines (Trend)
Range of Plunge Angles	0° - 90°
Class interval	10°
Class Alignment	Centered at 0°N
Kurtosis, k, of Smoothing Function	206
Half-width of Smoothing Function	±4.7°
Unweighted Calculation	

Frequency Statistics

Mode (Peak)	26.3%
Azimuth Range of Mode	95° - 105°
Smooth Peak	20.8%
Azimuth of Smooth Peak	97.5°
Expected Value, E	5.6%
Standard Deviation	7.7%
95% Confidence Level	>21.0%

The distribution has a preferred trend.

Figure 36: Rose diagram derived from trends of fold hinges found throughout the study area.

Figure 37: An example of some small, open, symmetric folds in the Goudplaats Gneiss.

Figure 38: An example of small folds which formed adjacent to the Matok Granite in the Goudplaats Gneiss as a result of the compression along the HRSZ.

3.5. Foliation:

Although foliation doesn't fall under brittle deformational structures, it was also measured. A stereographic projection (Figure 39) and a rose diagram of the foliation planes' orientations (Figure 40), show that NE and ENE-striking foliation is the most common, with a fairly large variation in dip angles. East-northeast is an azimuthal value analogous to the Limpopo Orogeny, an event that arguably had the largest structural influence on vast parts of the study area. The major strike directions of the foliation planes are almost identical to the major trends of the dolerite dykes in the area. For this reason it is likely that the dykes had exploited foliation by intruding parallel to the strikes of foliation planes in areas where NE and ENE-striking joints were uncommon at the time of emplacement. Hence, if dolerite dykes have an influence on the flow/occurrence of groundwater; foliation may be viewed as an indirect control in this regard.

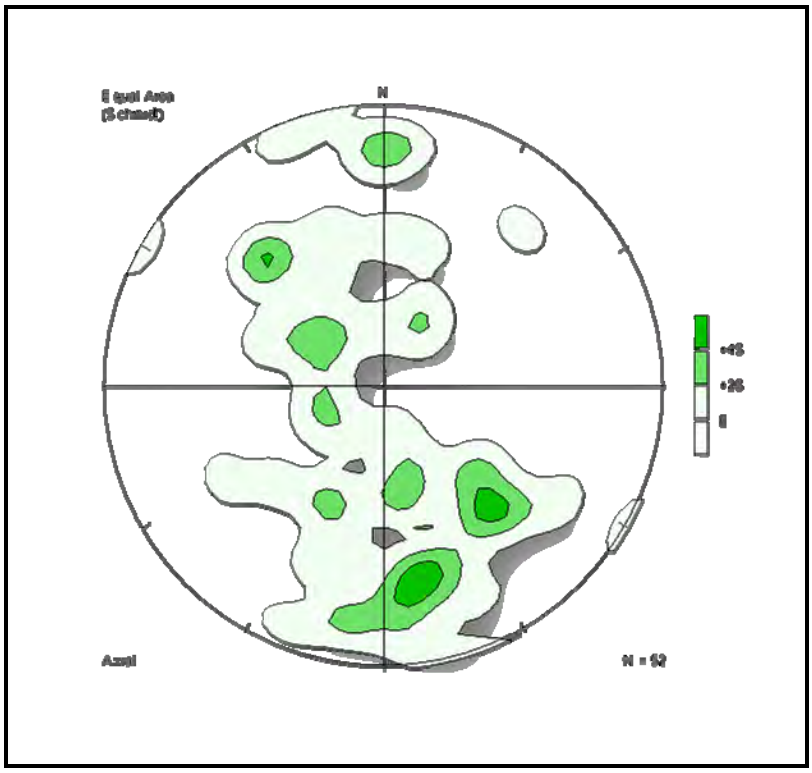

Figure 39: Density distribution of the poles to foliation planes.

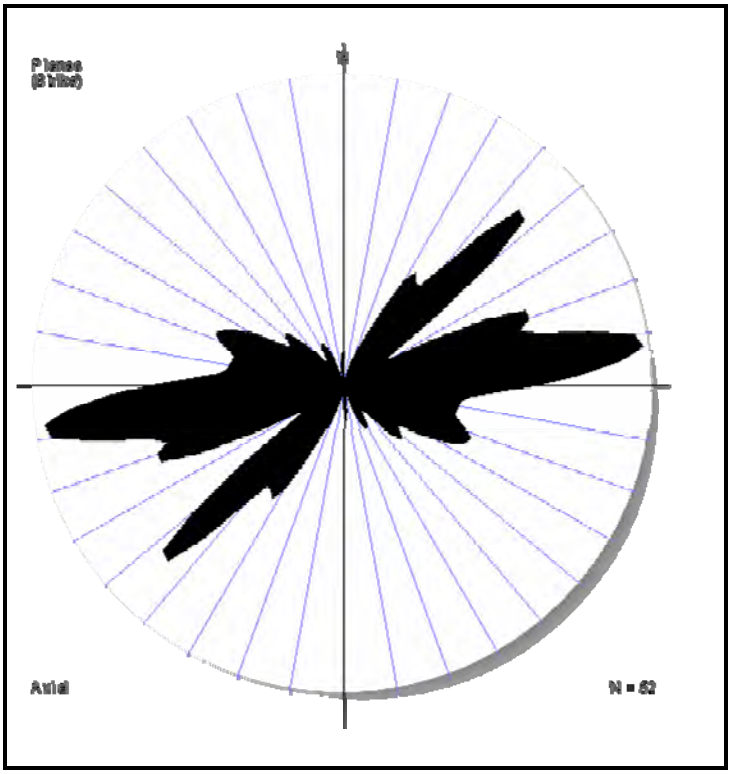

Figure 40: Rose diagram derived from the trends of foliation.

Counting Parameters	
Number of Data Points in Set	52
Number of Data Points Included	52
Type of Data	Planes (Strike)
Range of Dip Angles	0° - 90°
Class interval	10°
Class Alignment	Start at 0°N
Kurtosis, k, of Smoothing Function	206
Half-width of Smoothing Function	±4.7°
Unweighted Calculation	

Frequency Statistics	
Mode (Peak)	17.3%
Azimuth Range of Mode	80° - 90°
Smooth Peak	16.8%
Azimuth of Smooth Peak	82.5°
Expected Value, E	5.6%
Standard Deviation	4.7%
95% Confidence Level	>15.0%

The distribution has a preferred trend.

Figure 41: A picture showing strong foliation in gneisses near the township called Middelwater.

3.6. Dykes:

As with so many of the other geological structures in this study area, the trends of dolerite dykes observed are dominated by two directions, namely NE-SW and NNE-SSW (Figure 42). Such orientations measured from the field compare agreeably with interpretations based on regional aeromagnetic surveys and previous measurements of dykes seen in the literature review (refer to Figure 43 and section 3.6). Dolerite dykes may play a major controlling role on groundwater flow in this study area. Unjointed dolerite dykes can behave as aquicludes in some instances (Cook, 2003), but having the properties of an aquiclude doesn't restrict a dyke from having an influence on the orientation of groundwater flow. It might simply act as a type of barrier, which redirects water to flow or accumulate groundwater along its surface. Highly jointed dolerite dykes (e.g. those containing penetrating cooling joints) also make for good groundwater channels (Cook, 2003). The majority of the dykes observed in the field are less than 10m wide and therefore, according to Bromley et al. (1994) can be considered as good permeable conduits for groundwater. On the other hand, according to the current neotectonic stress-strain regime (NE-SW tension and NW-SE compression), the dykes are likely to be closed.

One of the complicating factors with regards to dolerite dykes in this study is the high spatial density within the dyke swarms. At a regional scale (on a small scale map) it is especially difficult to tell whether or not a borehole did actually strike a dolerite dyke or not. The only way to surely know whether dolerite dykes have a major influence on the flow or occurrence of groundwater in this specific study area is to analyze the borehole logs, which were not available at the time of printing this document. Presently available results are rendered inconclusive with regard to the influence of dolerites on groundwater at a regional scale. In the event of attaining borehole logs in the future, it is important to note the following attributes with regard to dolerites' influence on groundwater: 1.) To confirm whether a dolerite was struck or not (and at what depth); 2) the properties of the dolerite (weathering and jointing); 3) whether the borehole yielded water and if it did, at what depth, what transmissivity and what yield? A more in depth analysis could also consider the geometry, grain size and degree of weathering, as these also influence a dolerite's hydrogeological properties, but are regarded as being outside of this study.

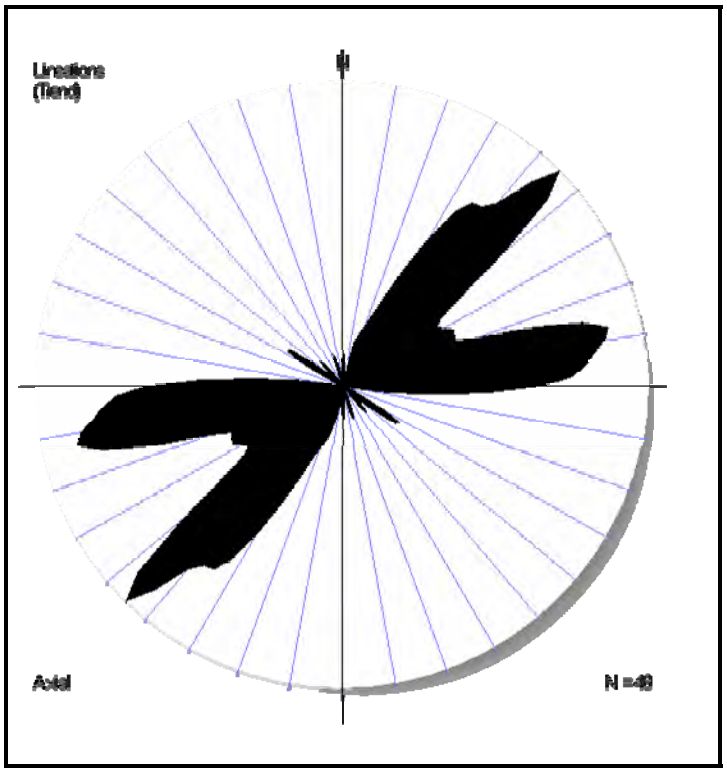

Counting Parameters	
Number of Data Points in Set	48
Number of Data Points Included	48
Type of Data	Lines (Trend)
Range of Plunge Angles	0° - 0°
Class interval	10°
Class Alignment	Centered at 0°N
Kurtosis, k, of Smoothing Function	206
Half-width of Smoothing Function	±4.7°
Unweighted Calculation	

Frequency Statistics	
Mode (Peak)	18.8%
Azimuth Range of Mode	45° - 55°
Smooth Peak	18.6%
Azimuth of Smooth Peak	45.0°
Expected Value, E	5.6%
Standard Deviation	4.9%
95% Confidence Level	>15.3%

The distribution has a preferred trend.

Figure 42: Rose diagram derived from strikes of dolerite dykes in the study area.

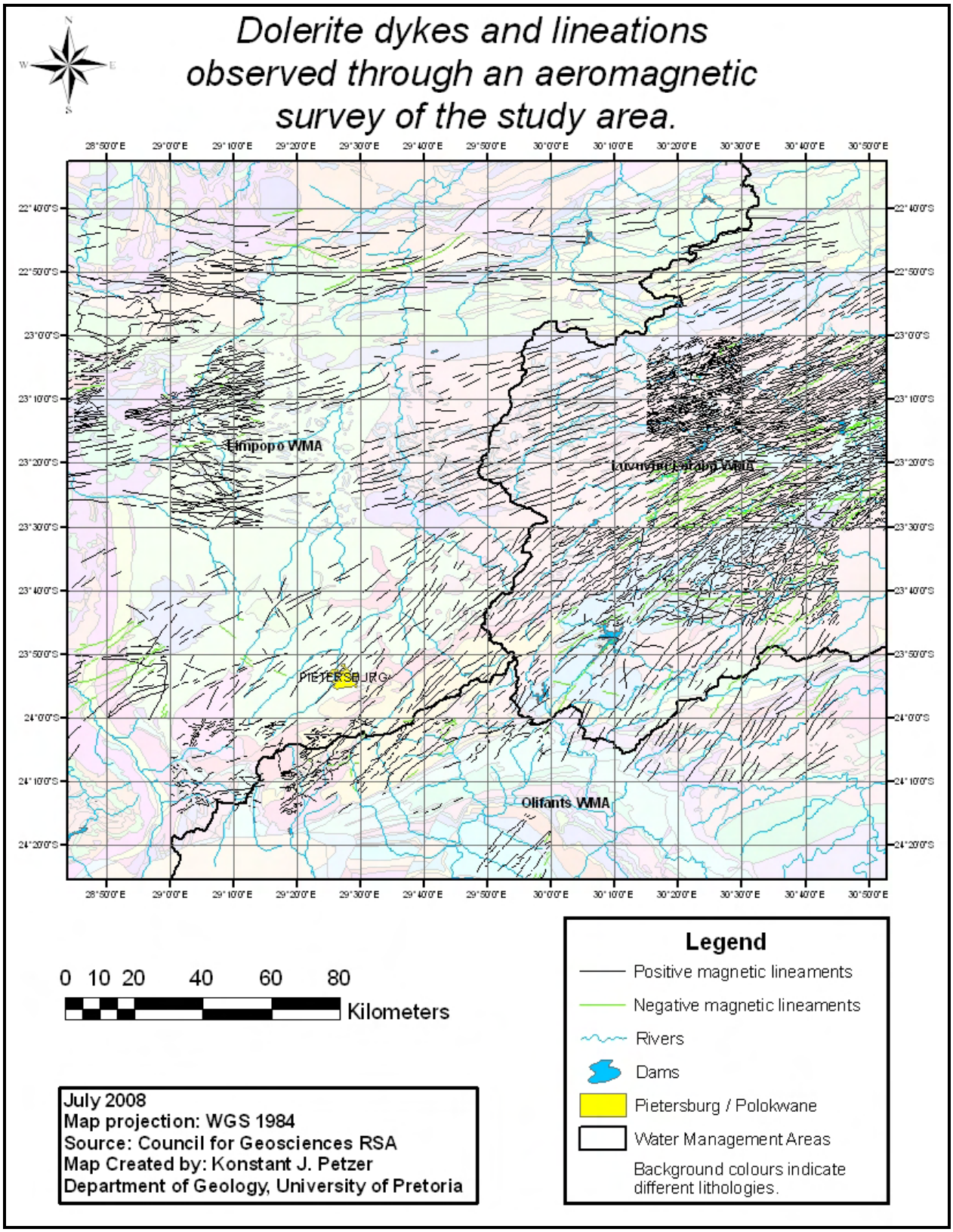

Figure 43: A map indicating the dolerite dykes and other lineaments that were observed through an aeromagnetic survey of the study area done by the Council for Geosciences. Not all areas of the map were covered at the same resolution. Note the dominant NE and NNE trends.

Figure 44: A 60cm wide, dolerite dyke with sharp edges (256˚, 84˚ NW), implying that it intruded into one of the pre-existing joints with the same orientation found in the area.

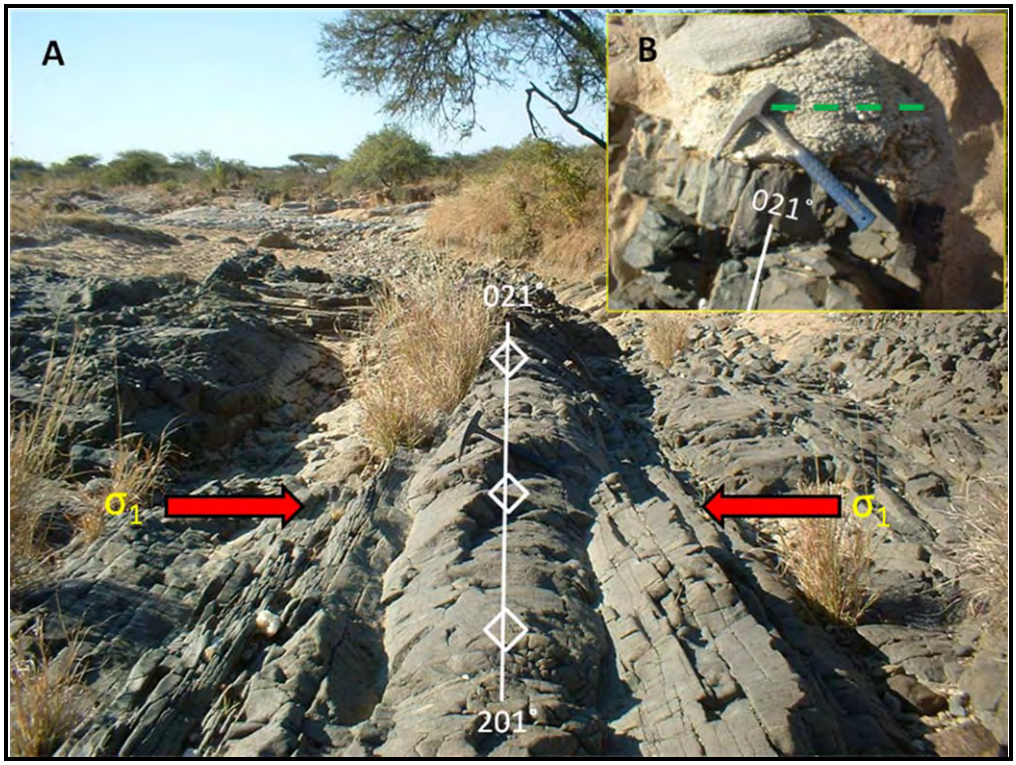

Figure 45: (A) A dolerite sill with outcrop dimensions of about 60m x 40m (long axis trending 152˚). This photo was taken along an anticline in the dolerite (hinge: trend 021˚, plunge 02˚, λ = 8m) which probably formed as a result of primary folding (when the dolerite was still molten), because the pre-existing gneiss surrounding the area seems to be unaffected by the σ_1 compression which caused the folds. (B) In fact the surrounding gneiss shows foliation (indicated by green stipple line) which strikes approximately perpendicular to the trend of the folds in the dolerite.

3.7. Summary of strikes/trends:

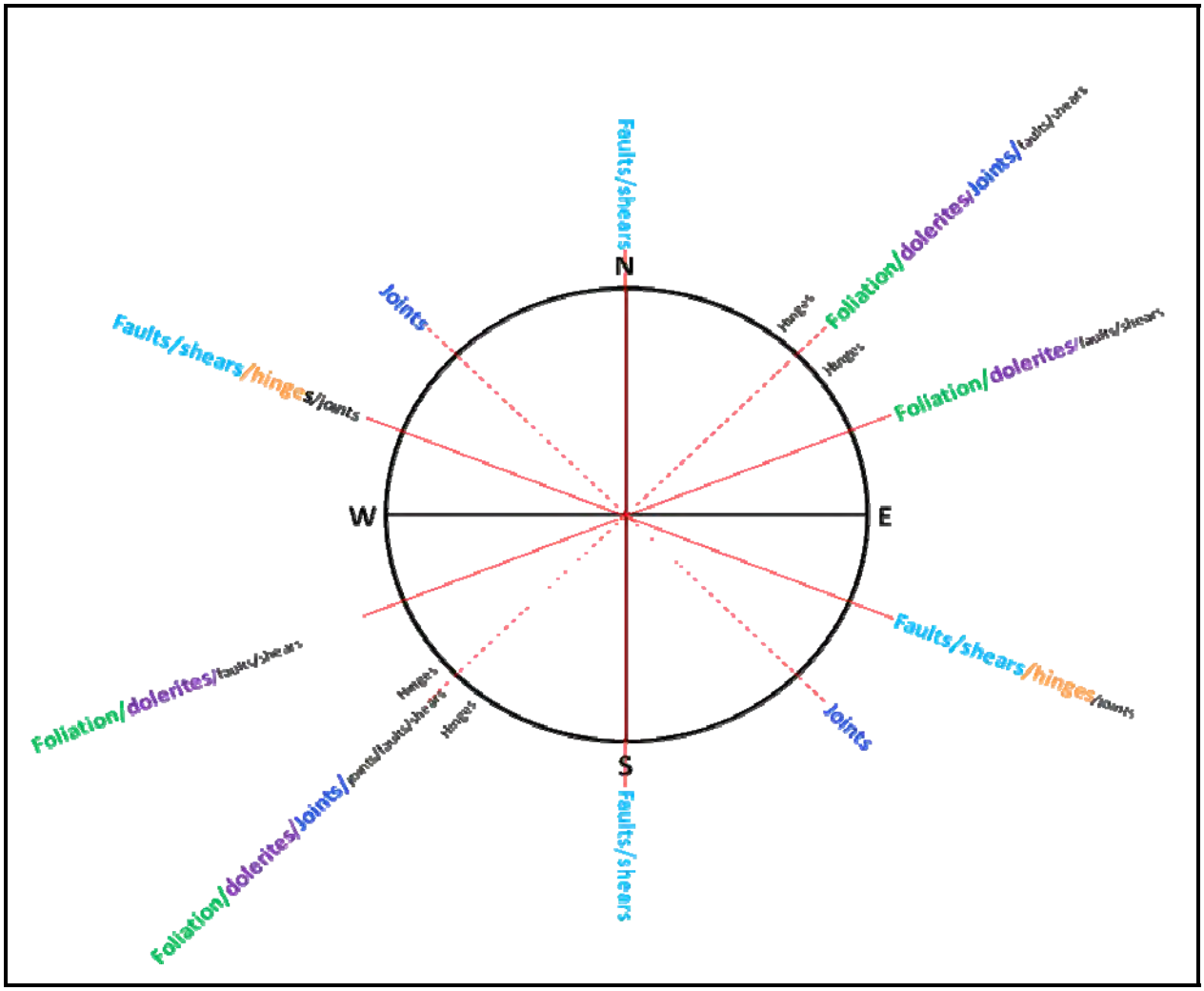

Figure 46: A summary of the strikes/trends of structures observed in the field.

3.8. Lithological Contacts:

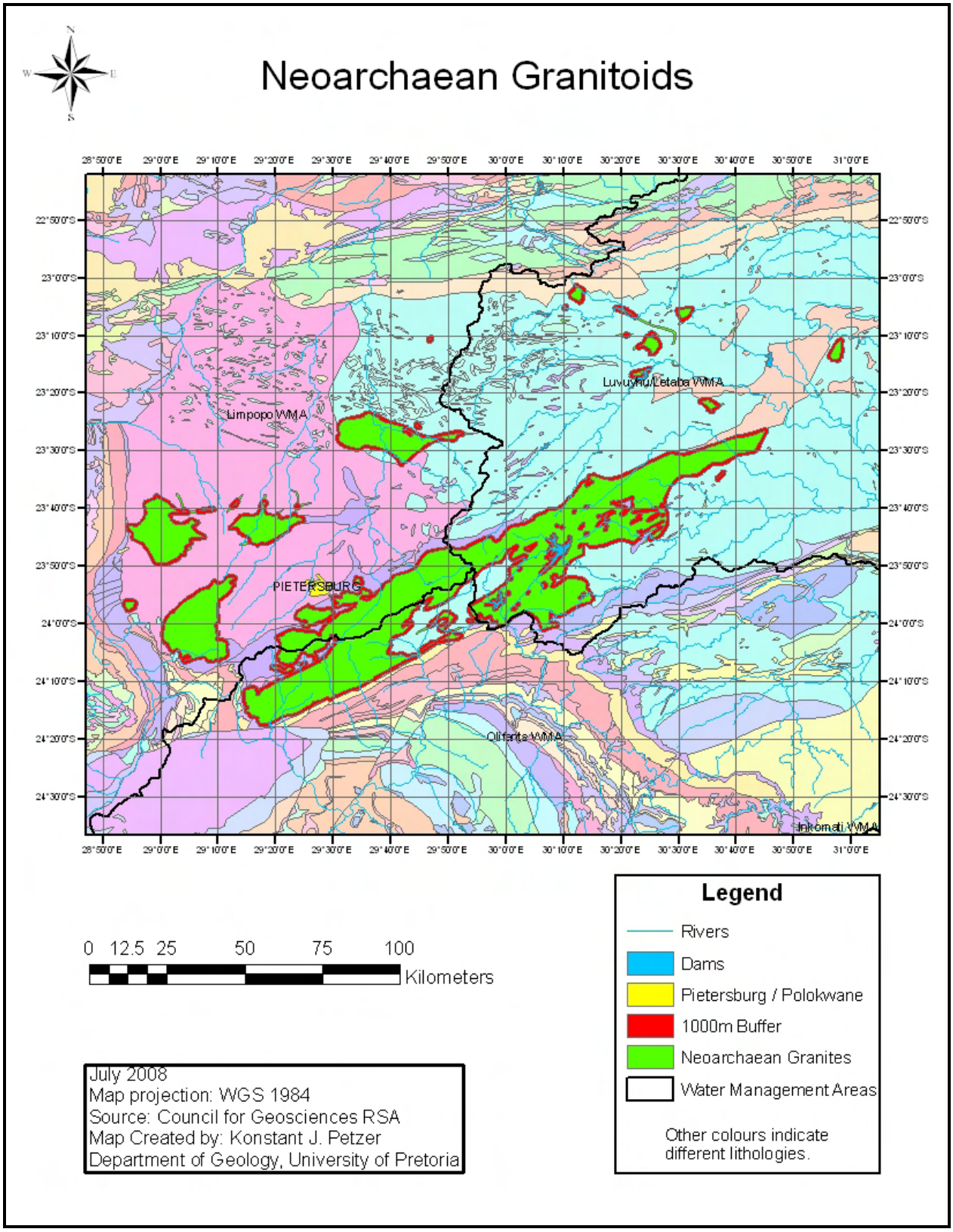

Figure 47: A map indicating the location of the Neoarchaean granitoids in the study area and a 1000m buffer (500m inside & 500m outside) around their contacts.

Table 5: A table showing the average T and Q values for different groups of boreholes in relation to their spatial distribution relative to Neoarchaean Granitoids.

Property of borehole	Boreholes in Neoarchaean Granitoids	Boreholes in the 1000m buffer at Neoarchaean granitoid contacts	Boreholes outside of the Neoarchaean Granitoids
Mean Average Transmissivity (T-logan) (M^2/d)	25.37	55.52	42.53
Mean Average Sustainable yield (Q) (L/sec./24hr)	0.77	1.57	1.19

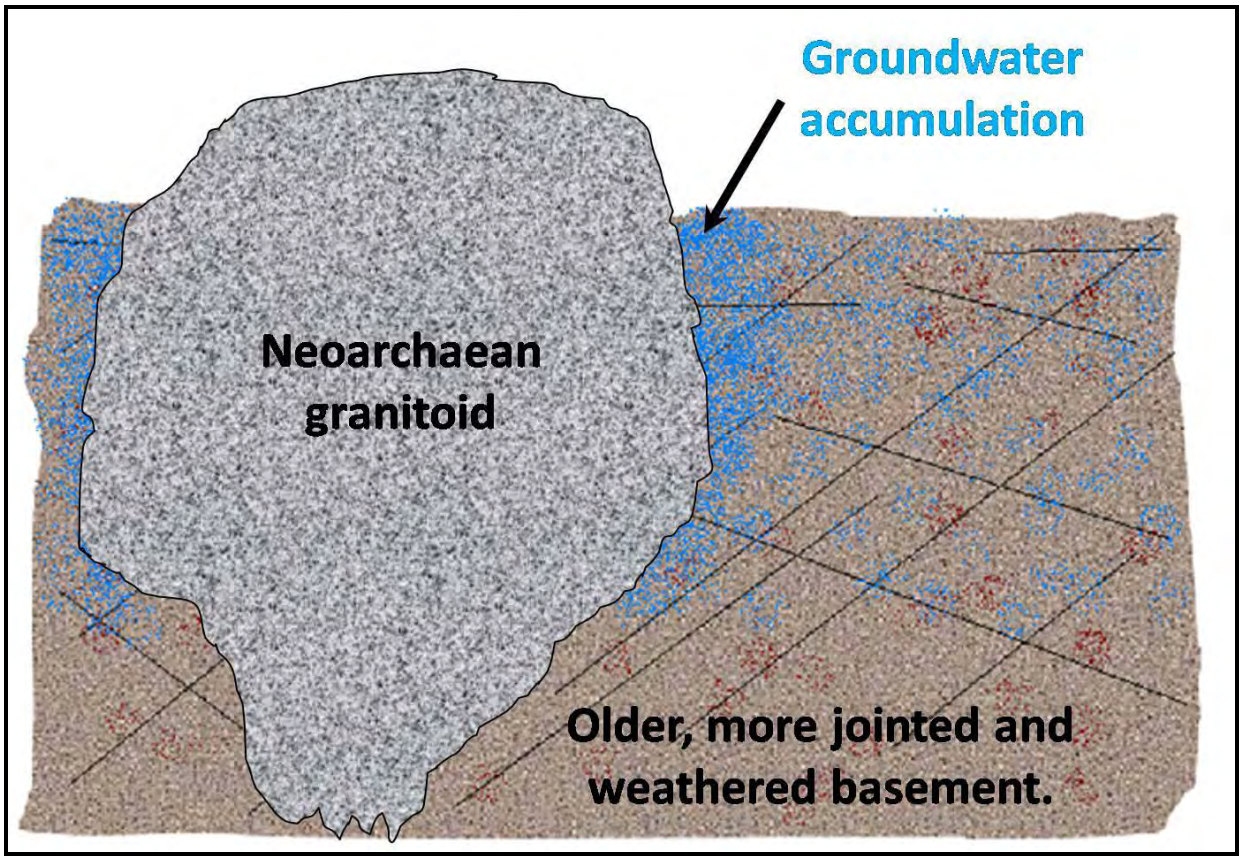

Figure 48: Groundwater accumulation related to the lithological contacts between Neoarchaean granitoids and older basement rocks in the study area.

As hypothesized, the averages of both the transmissivity- (T) and yield (Q) values are ranked in the following manner based on their lithological location: Firstly, the highest average T and Q values were obtained at the contacts between the Neoarchaean granitoids and the surrounding basement rocks. This is because groundwater can move relatively freely through the weathered and jointed old basement lithologies, but dams up against the post-tectonic, unweathered Neoarchaean granitoids which are less penetrable. The second highest average T and Q values were obtained from the surrounding old basement lithologies and the lowest averages came from within the Neoarchaean granitoids.

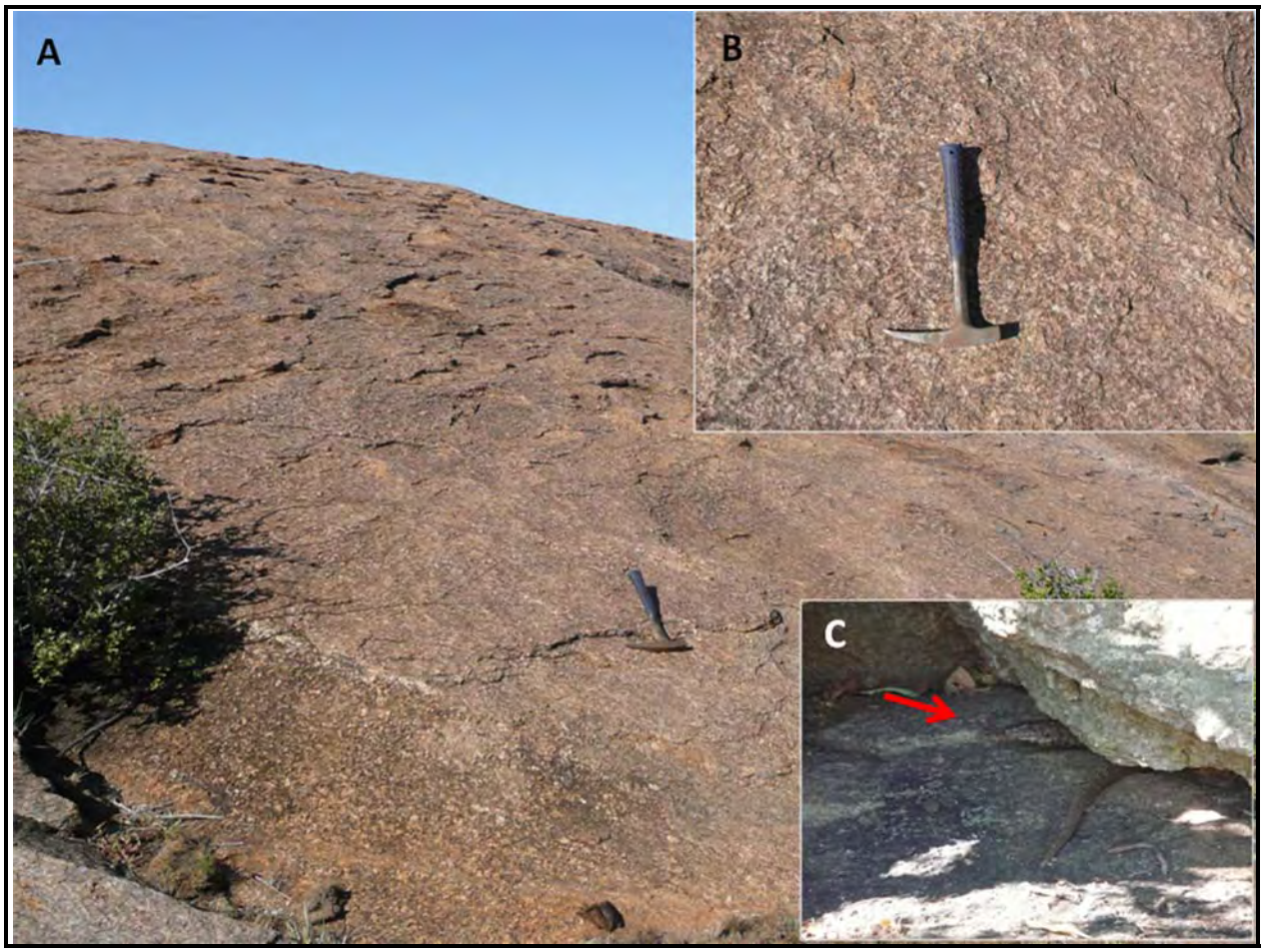

Figure 49: (A) An example of a Neoarchaean Granite, which only shows a dilatational pressure-release surface, but not any tectonically induced joints. (B) A close-up look at the same granite still doesn't indicate any joints. (C) Some animals use the dilatational cracks in the granite as a shelter.

3.9. Groundwater flow/occurrence:

From Figure 50 to Figure 55, the spatial interpolation of the inverse distance weighted yield and transmissivity values were plotted for different portions of the study area. When comparing these interpolations with the brittle geological structures that have been observed in the field, there doesn't seem to be a strong spatial correlation, at least not on a regional scale. The following observations can be made from slight local scale trends in the interpolated plots: Firstly, in Figure 50 there seems to be a slight NE-trend in the interpolated transmissivity values near the centre of the map. Although this trend is not bound to a specific lithology, it does match the trend of the rivers, the major strike direction of joints (Figure 19) and the trend of the sub-horizontal cluster of joint intersections (mentioned in section 4.1). A similar relationship can be seen on the same area of the map in Figure 51 in which the interpolated sustainable yield values form one very slight trend orientated approximately NNE-SSW. Another observation is the fact that the Pietersburg Greenstone Belt (seen only as an outline in Figure 52; verify location with Figure 5) definitely has low transmissivity compared to the lithologies north of it (Figure 15 contains many boreholes located in the PGSB to confirm this statement). Another approach was taken in Figure 56 by plotting a three-dimensional model of the transmissivities of a part of the study area with a good spatial distribution of boreholes over a corresponding geological map. Although a slight trend in higher transmissivity could be argued around a portion of the HRSZ, the three-dimensional model created does not correlate well with the area's structural geology at a regional scale.

After the disappointment of not finding a strong structural control of groundwater at a regional scale, it was decided to take a closer look at the specific boreholes that did possess high Q-values. A query was run on the borehole database to find the following boreholes with Q > 6L/sec/24h: H04-0848, H04-0905, H04-0962, H04-0988, H04-1022A, H07-1061, H10-0548, H10-0657, H16-0358, H16-0426, H16-0471, H16-0485, H16-0551, H16-0580. The properties of these boreholes, in terms of their localities, were investigated to look for a reoccurring similarity. Lithologically, many of these boreholes are located on or near to NE-SW trending dolerite dykes (must be confirmed with borehole logs in the future). NNE-SSW and NE-SW striking faults were also observed at a few of these boreholes. Other than the structural controls on groundwater, two possible other controls were also observed. Firstly many of the high-yielding boreholes are located in the alluvium of rivers. It is no surprise that this type of weathered environment can act as a good aquifer.

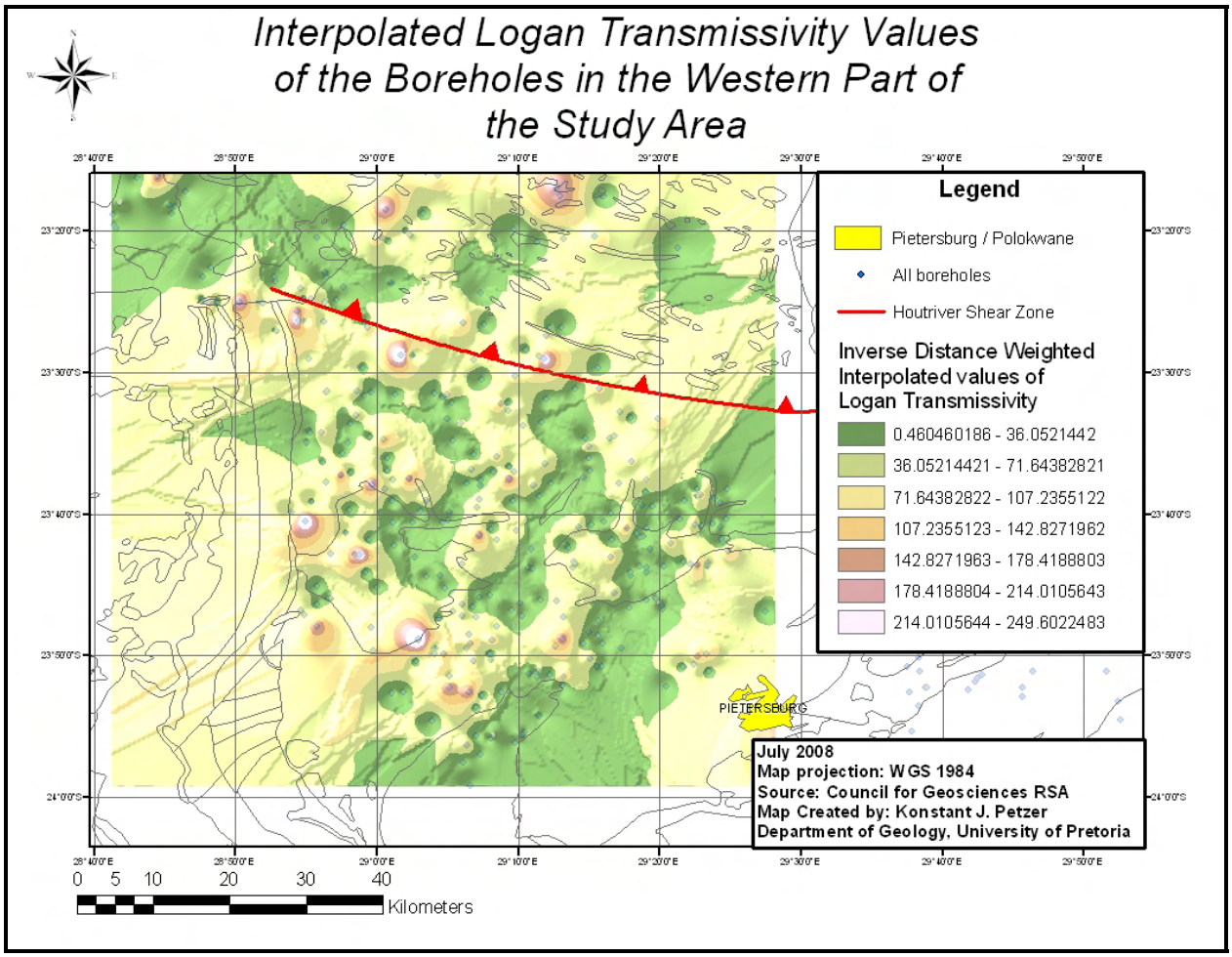

Figure 50: A map of the interpolated (inverse distance weighted) Logan transmissivity values of the western part of the study area.

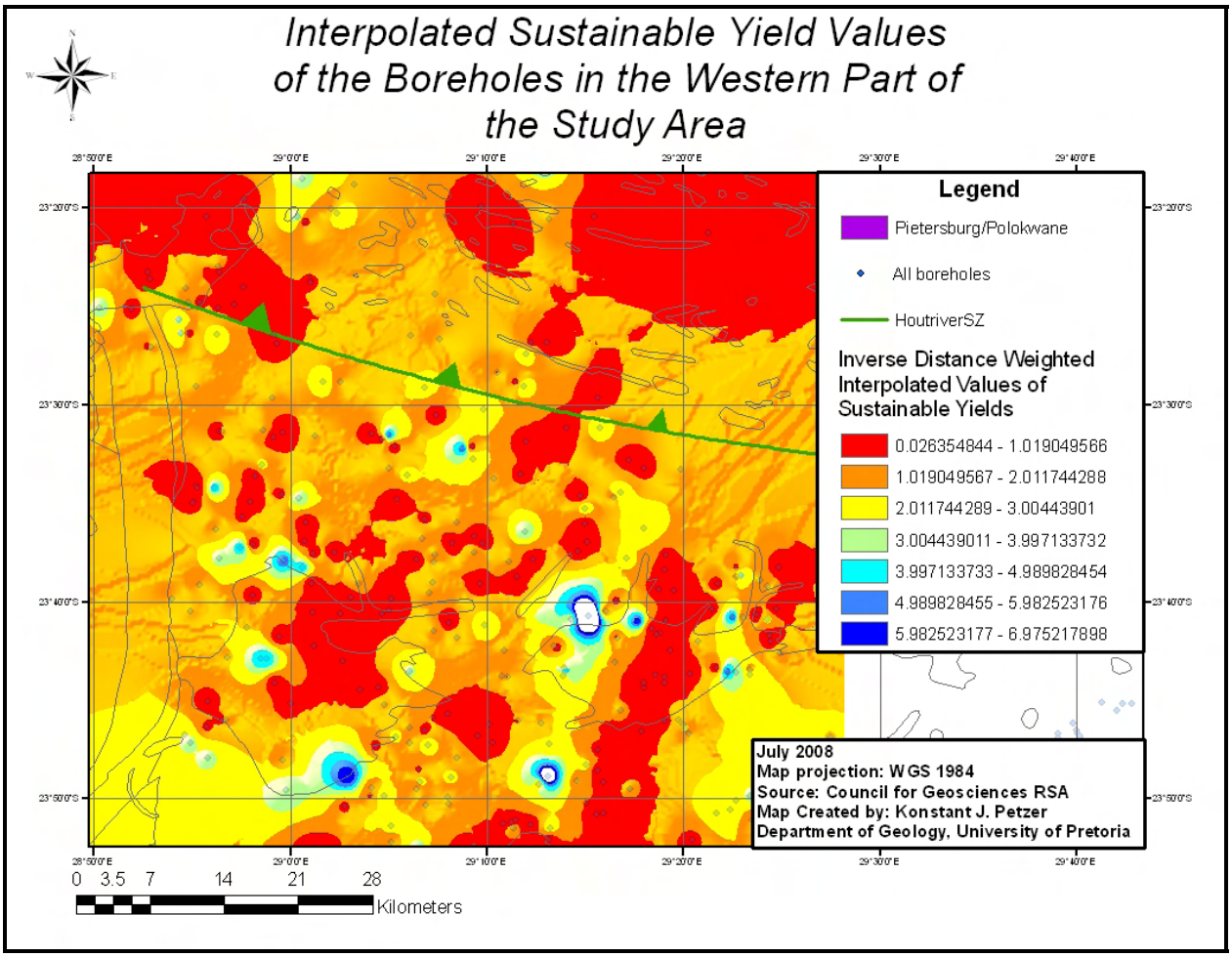

Figure 51: A map of the interpolated (inverse distance weighted) sustainable yield values of the western part of the study area.

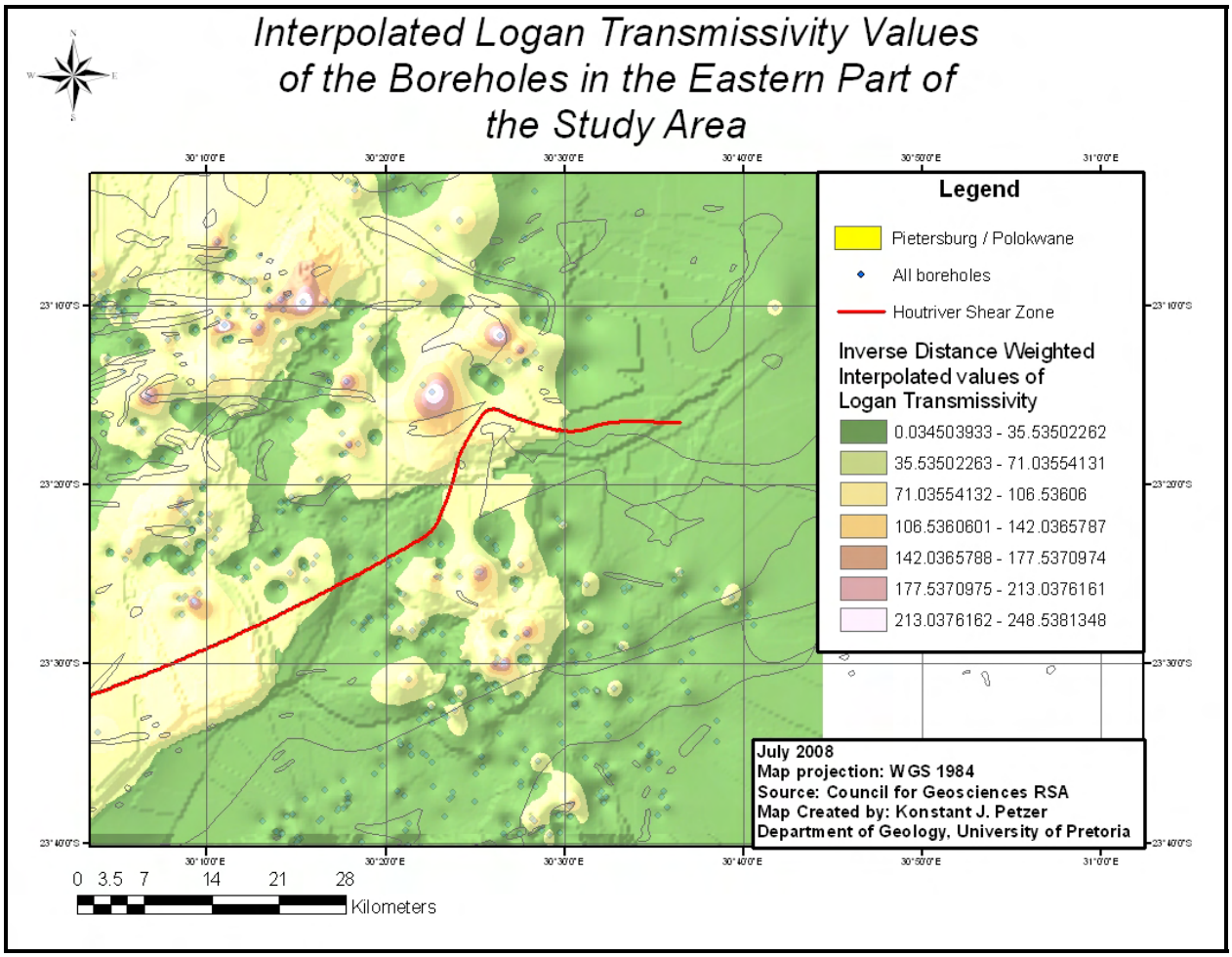

Figure 52: A map of the interpolated (inverse distance weighted) Logan transmissivity values of the eastern part of the study area.

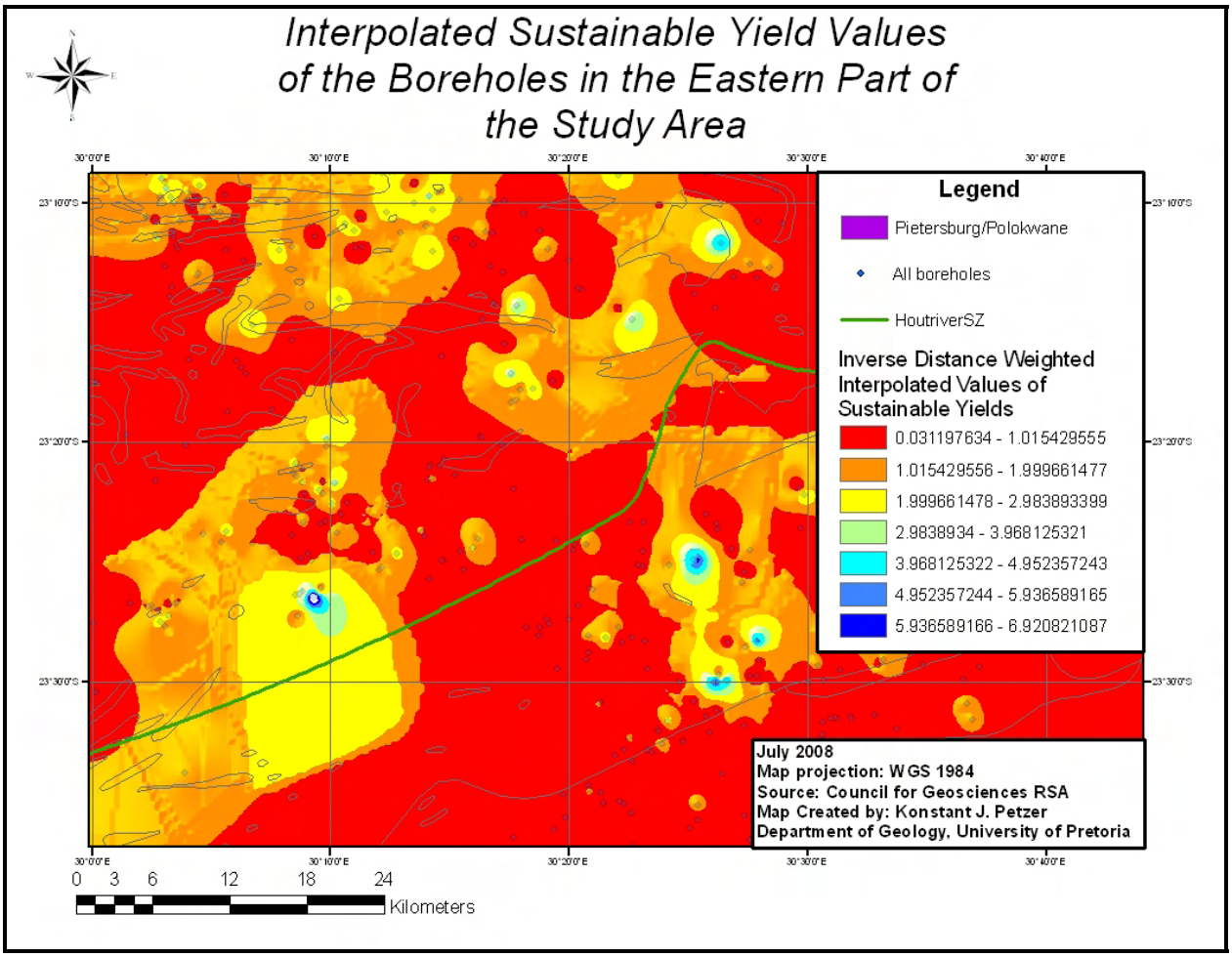

Figure 53: A map of the interpolated (inverse distance weighted) sustainable yield values of the eastern part of the study area.

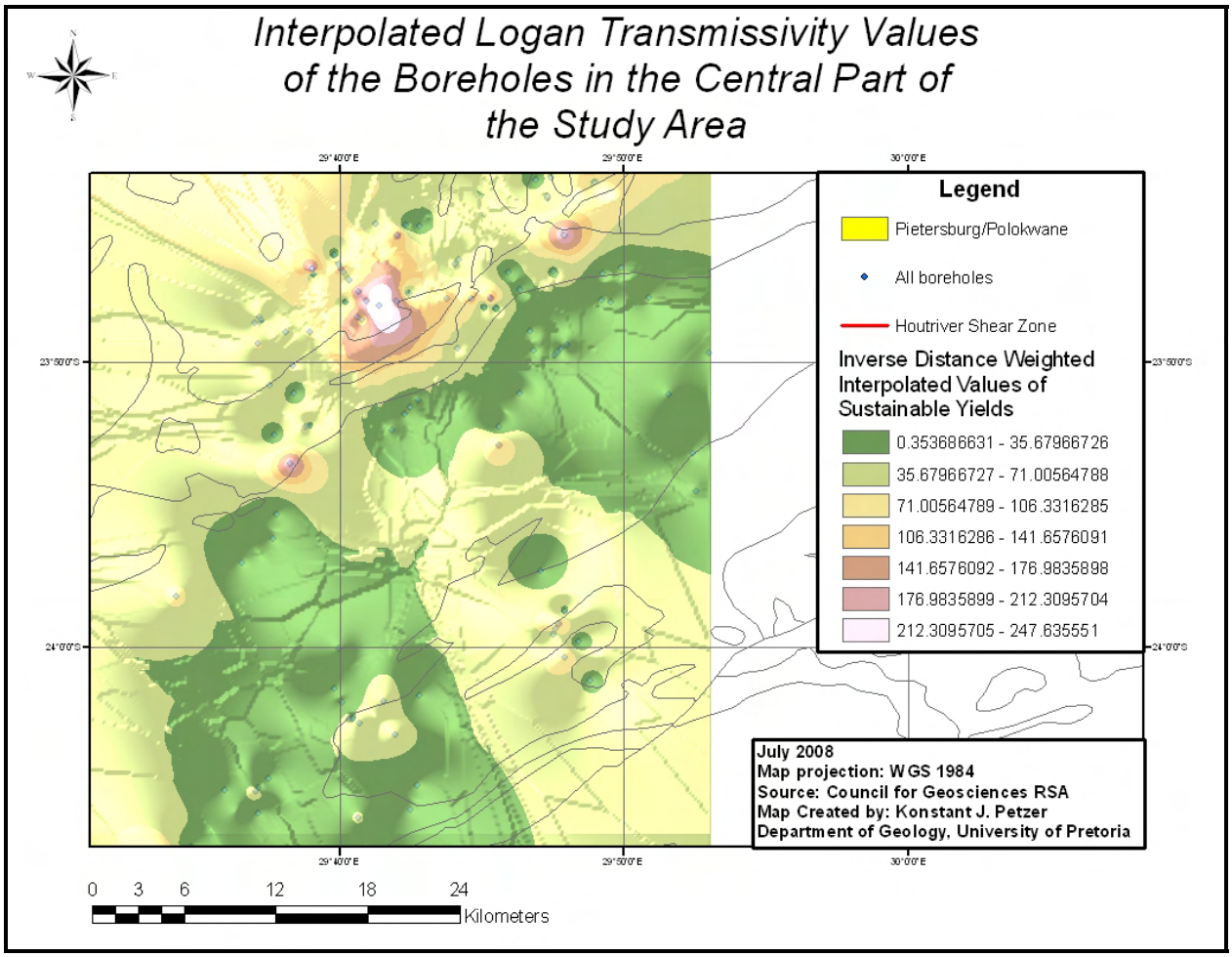

Figure 54: A map of the interpolated (inverse distance weighted) Logan transmissivity values of the central part of the study area.

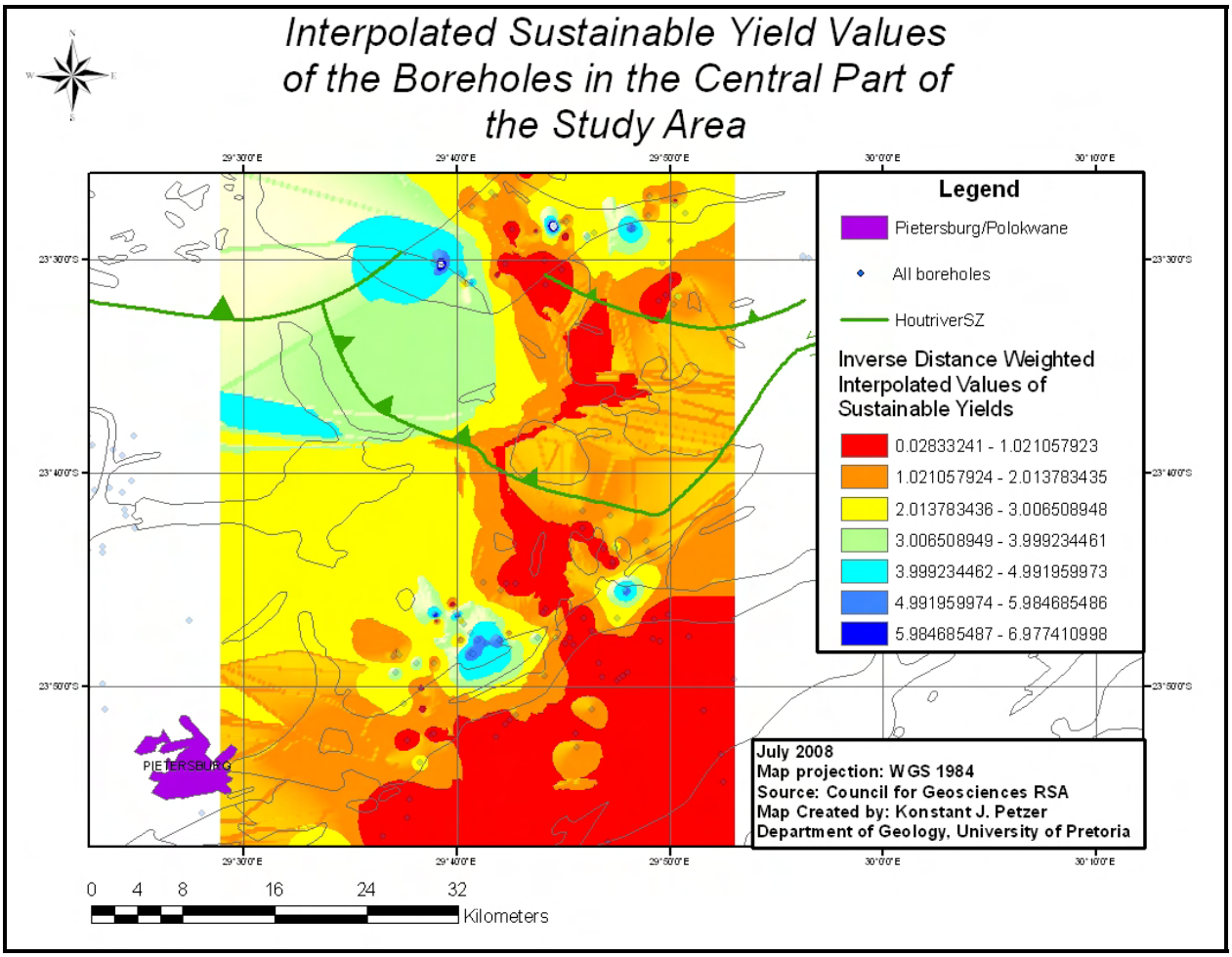

Figure 55: A map of the interpolated (inverse distance weighted) sustainable yield values of the central part of the study area.

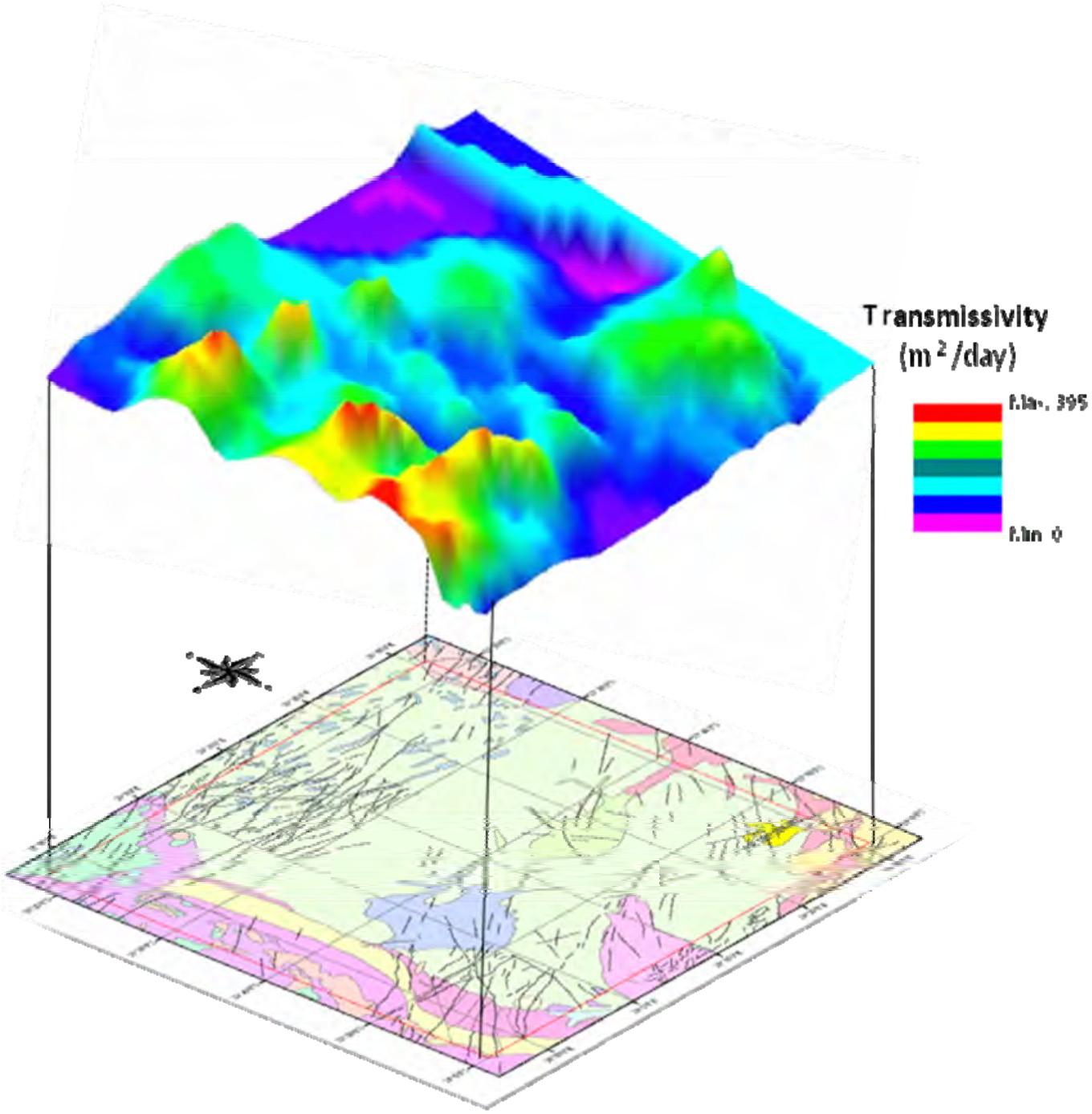

Figure 56: A Three-dimensional model of the Logan Transmissivities from a part of the study area with a good spatial distribution of boreholes, superimposed onto a corresponding geological map of the area. Although the patterns on the three-dimensional model do not seem totally random, they cannot be clearly correlated with structural geology at a regional scale. The three-dimensional model was created using Rockworks 2006 © software.

3.10. Surface Drainage Patterns:

When looking at Figure 57, one can draw a few conclusions based on the surface drainage patterns of the study area. Firstly, the density of rivers in WMA2 is higher than the spread out distribution of rivers in WMA1. There might be more rivers in WMA2 due to the greater annual rainfall in this area. Furthermore, WMA1's drainage pattern is dendritic, whereas drainage patterns of the rivers in WMA2 vary from dendritic to blocky (caused by joints). Rivers in WMA1 mainly trend in the following directions: N-S, NE-SW and NW-SE and rivers flowing parallel to the first two directions mentioned are especially long and continuous. NE-SW is also a major trending direction of rivers in WMA2, along with E-W and NNW-SSE (this direction becomes more common as one move from west to east in WMA2). For the most part, the rivers in the study area flow sub-parallel to the major joint orientations found at that location, especially where the joint intersection lineations form sub-horizontal clusters (refer to "Joint intersection lineations" under section 3.2 and compare Figure 57 with Figure 19).

The trends of the rivers mentioned above also compares well with the rose diagram constructed for faults (Figure 28). In areas where the rivers don't flow sub-parallel to the major joint directions, there are still at least some joints striking in the same direction as the flow of the river albeit a so called "major strike direction" or not. Despite not finding very strong correlations between groundwater flow/occurrence in the previous sections, structural geological controls on a few of the surface drainage patterns are unmistakable even though the influences are mainly seen at a local scale (see Figure 58). Unfortunately, the structural controls seen on the surface are not necessarily exactly an indication as to what is happening underground. For example, the three-dimensional strain mentioned in section 2.2 can cause joints/faults to deviate from the "standard" joints/faults described in Anderson's Theory, which produces a difference in joint patterns between the surface and underground (see Figure 59 and Figure 60). Lastly, other controls such as topography also have an influence on surface drainage patterns. For example, one finds closely-spaced, short rivers on the escarpment next to the Lowveld, as compared to longer, widely-spaced rivers of the flat plains.

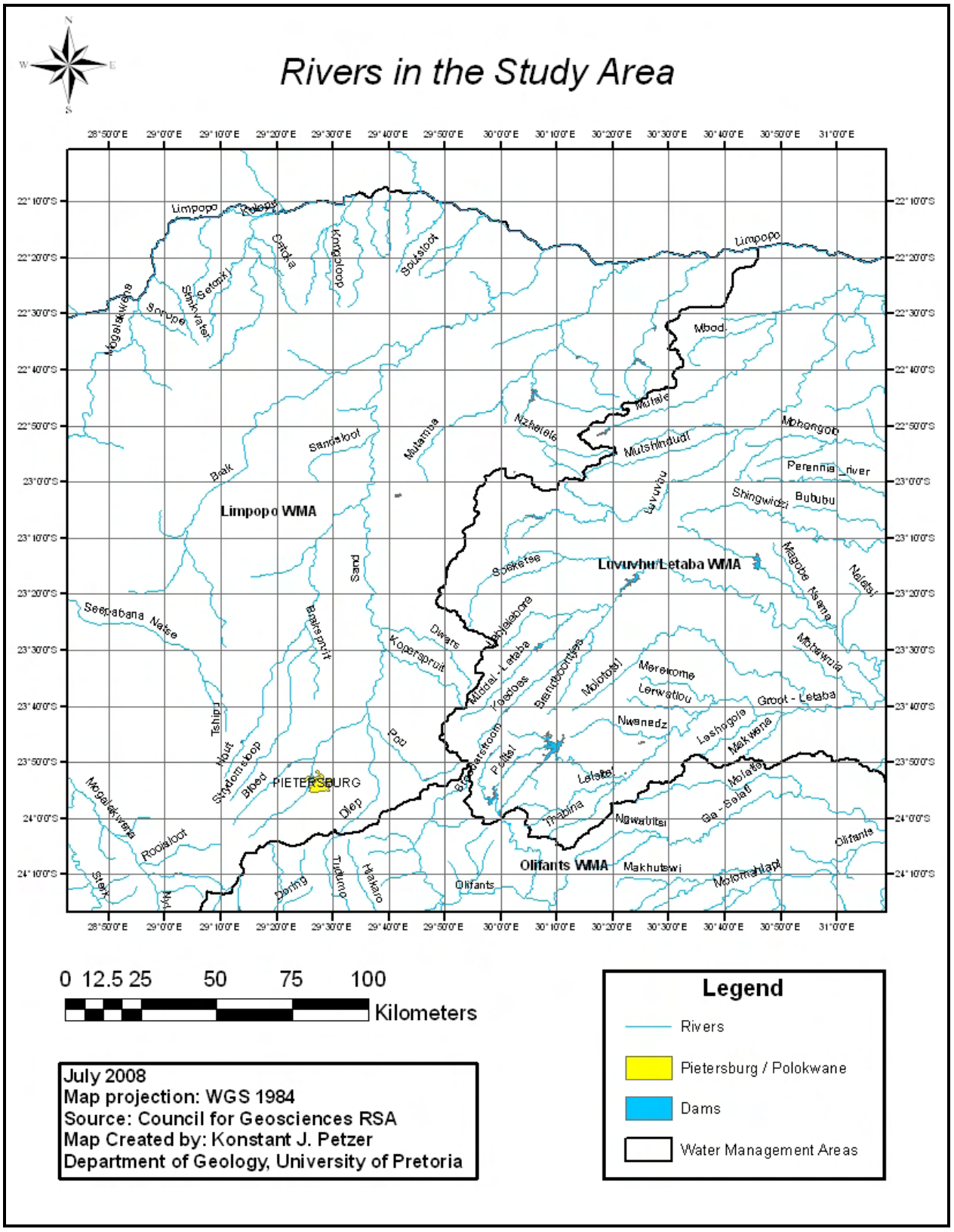

Figure 57: A map indicating the surface drainage patterns of the study area.

Figure 58: A Google Earth satellite image taken near the Giyani Greenstone Belt showing NNE, NE and lesser NW trending joint sets. Note that the flow of the river is guided by the underlying joints in most sections.

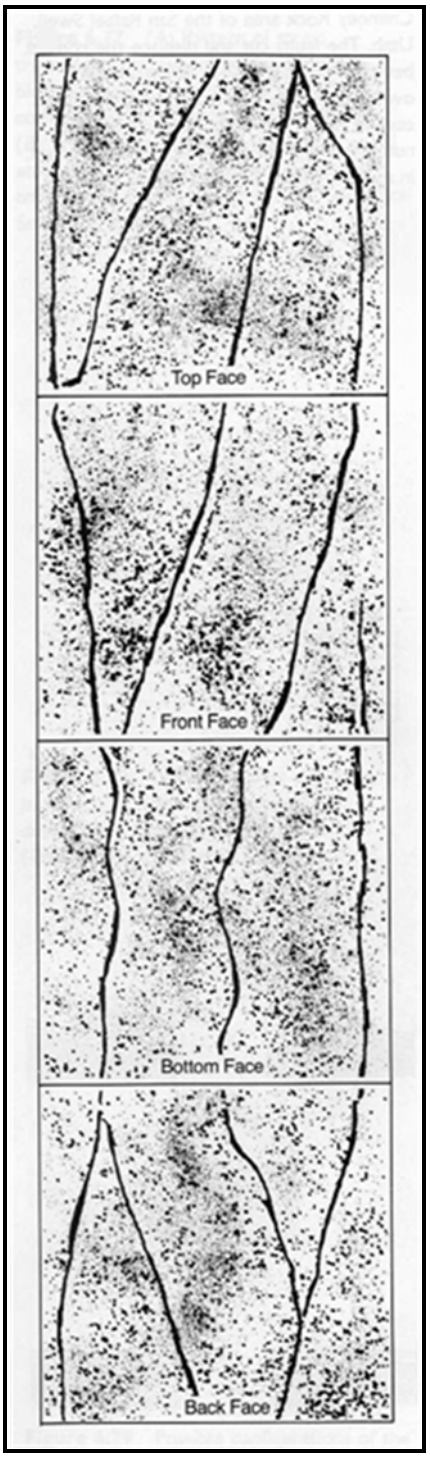

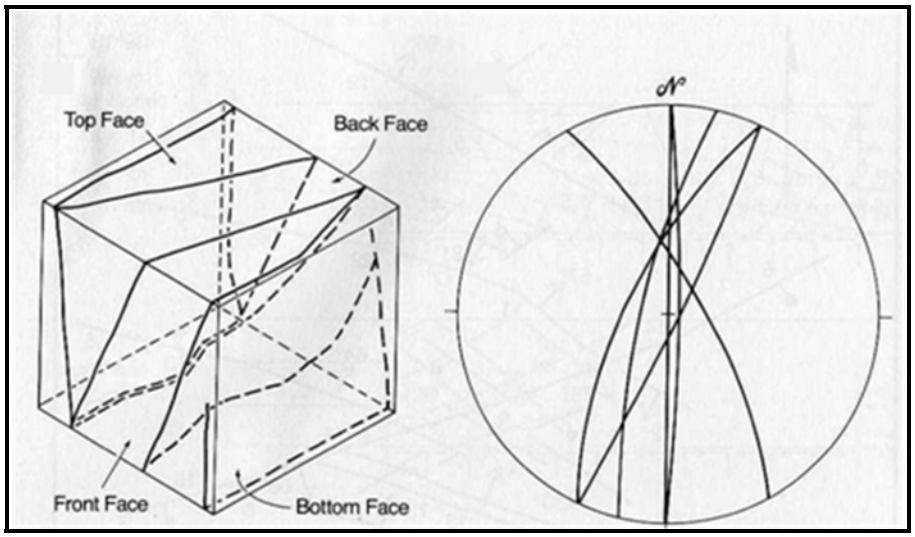

Figure 59: A three-dimensional illustration and an associated stereographic projection of fault patterns produced in rock subjected to three-dimensional strain. From Reches and Dieterich, 1983.

Figure 60: The traces of faults correlating to the fault patterns seen in Figure 59 Note that the fault pattern changes with depth and might mean that surface drainage patterns (which often follow faults and joints) might not give a good indication as to the patterns in groundwater conduits at depth. From Reches and Dieterich, 1983.

4. CONCLUSION:

After investigating all the results from this study, no strong spatial correlation between structural geology and groundwater can be identified at a regional scale. It is believed that the extremely old age (starting from the middle of the Archaean Eon) of the rocks in the area is the major factor which is indirectly responsible for this poor correlation. Numerous tectonic and magmatic events have had an influence on the geology of the study area which have ultimately brought about a structurally complex terrain. The complexity of the basement's structural geology in the Limpopo Province makes it difficult to isolate the effects of a specific set of structures on the flow and occurrence of groundwater. Nevertheless, the following observations regarding the presence of water in the basement rocks of the Limpopo Province have been made.

Firstly, the influence of the neotectonic stress direction on the presence of groundwater appears to be negligible, at least at a regional scale. With a dominant NE-SW extensional regime one would have expected to find more favourable groundwater conduits striking NW-SE, but this hypothesis was rejected. When looking at surface water, it was interesting to find that in areas with preferred clusters of sub-horizontal joint intersections (figures in appendix), the rivers in those areas flow parallel to the trends of such clusters (see section 4.1 "Joint intersection lineations").

Unlike the other groups of joints, those inclined at angles ranging from eighty to ninety degrees did show preferred orientation trending NW-SE. Many of these joints might well have formed due to the neotectonic stress regime. However, as mentioned before, the occurrence of groundwater does not seem to be influenced by neotectonic stess to the extent that an associated preferred orientation of proven conduits are found in the area.

When examining the shallow-dipping joints (those inclined from zero to forty-five degrees), it was found that the distribution of these joints is well spread out over the entire study area. Whereas some of the shallow-dipping joints could have formed due to dilatation (i.e. pressure release as a result of erosion or plutonism), it is believed that many of these joints are actually tectonically induced, suggesting that the whole study area was likely subjected to compression at one stage or another. This being said, many of the brittle structures that might have been favourable groundwater conduits long ago could subsequently have been closed up.

Despite the fact that NW-SE trending joints were initially believed to be the most promising targets for groundwater (due to their orientation relative to the neotectonic stress direction), the importance of the other major direction observed, NE-SW, cannot be overlooked. Joints striking NE-SW were likely reactivated during successive tectonic events

(for example the N-S extension during later Karoo times) and lie parallel to one of two strong preferred orientations (NE-SW and NNE-SSW) displayed by dolerite dykes in the area. Unfortunately, not even those properties resulted in groundwater conduits showing dominant NE-SW strike directions.

From the results it is clear that the tectonic structures (including large structures like the Hout River Shear Zone) and dolerite dykes from the study area produced hardly any positive conclusions in terms of groundwater exploration on a regional scale. Thus, conclusions regarding the influence of weathering and lithology on groundwater occurrence are also recorded below.

One part of the investigation which yielded positive proven results involves the relationship between groundwater occurrence and the lithological location relative to Neoarchaean granitoids. By investigating the following three lithological locations: 1) Inside Neoarchaean granitoids; 2) the contacts between Neoarchaean granitoids and the surrounding older basement rocks; 3) inside the surrounding basement rocks, it was shown that the highest averages of both the transmissivity- (T) and yield (Q) values were obtained at the contacts between the Neoarchaean granitoids and the surrounding basement rocks (See Table 5.) This phenomenon occurs because groundwater can move comparatively freely through the weathered and jointed old basement lithologies, but dams up against the post-tectonic, unweathered Neoarchaean granitoids which are less penetrable (Figure 48). The second highest average T and Q values were obtained from the surrounding old basement lithologies and the lowest averages came from within the Neoarchaean granitoids themselves.

Unsurprisingly, boreholes located in the alluvium of rivers produced relatively higher yields and transmissivities of groundwater. Where the law does not restrict it, boreholes close to rivers are often promising targets when drilling for water.

In conclusion, the structural geology in the basement lithologies of the Limpopo Province of South-Africa does not have a clearly identifiable influence in terms of spatial patterns in groundwater flow and occurrence at a regional scale. Groundwater targets created through weathering rather than tectonics are evidently more easily recognized. Structural controls on groundwater in the granitic aquifers from this specific area are not totally negligible, although it is believed that such influences will be better identified through intensive local scale investigations.

5. SUGGESTIONS FOR FURTHER STUDY:

In order to better identify the structural controls on groundwater in the area it is suggested that more intensive studies be conducted in much smaller areas. In this way, the local scale influences of structures on groundwater could be easily isolated and identified. If the budget allows it, it is also recommended to change the order of investigation. In other words, to map geological structures first and then drill at a specific location/structure to prove or disprove its hypothesized influence on groundwater instead of relying on interpolated groundwater data between existing boreholes. Furthermore, more emphasis should be placed on joint density (spacing between joints), aperture width and interconnectivity instead of only relying on the three-dimensional orientation and locations of joints.

Unfortunately not enough borehole logs were available at the time of submission of this thesis. To better understand the influence of dolerite dykes on groundwater the borehole logs can be investigated to see whether dolerite was struck at specific boreholes and whether water was encountered above, below or within a dyke and what types of yields were acquired. Such data can then be statistically analysed. As mentioned before, the degree of weathering, geometry and grain size of dolerites can also be recorded and analysed.

According to the information gathered through this study, the most suitable groundwater targets for further investigation are recommended to meet the following criteria. Where sub-horizontal clusters of joint intersects correlate with the strike direction of rivers in that area: Drill in highly weathered features (preferably ones that formed under tensional conditions) striking parallel to these clusters/rivers and if possible at the contacts between different lithologies.